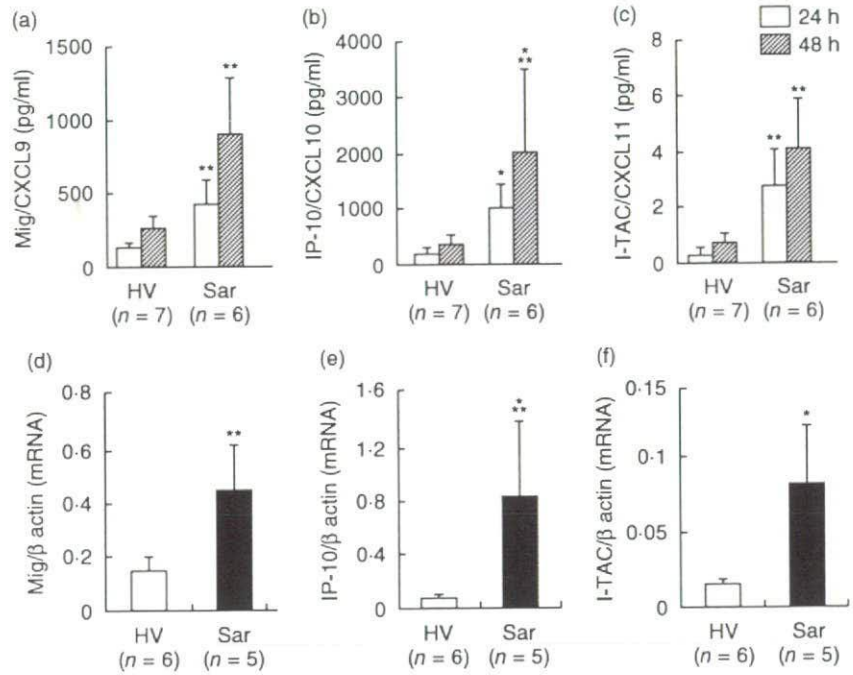

Fig. 5. Expression of monokine induced by interferon γ (Mig)/CXCL9, interferon-inducible protein-10 (IP-10)/CXCL10 and interferon-inducible T cell α-chemoattractant (I-TAC)/CXCL11 by alveolar macrophages harvested from patients with sarcoidosis. Alveolar macrophages were harvested from healthy volunteers (HV) or patients with sarcoidosis, and cultured without stimulation for 24 or 48 h. The supernatants were harvested, and the concentrations of Mig/CXCL9 (a), IP-10/CXCL10 (b) and I-TAC/CXCL11 (c) were measured with enzyme-linked immunosorbent assay (ELISA). Data are shown as mean ± standard deviation (s.d.). Total RNA was also extracted from alveolar macrophages in HV or patients with sarcoidosis. The real-time quantitative reverse transcription–polymerase chain reactions (RT–PCRs) for Mig/CXCL9 (d), IP-10/CXCL10 (e) and I-TAC/CXCL11 (f) were performed as described in Methods. Data are shown as mean ± s.d. of relative expression compared to β-actin. $^{*}P < 0{\cdot}005$ *versus* HV groups, $^{**}P < 0{\cdot}01$ *versus* HV groups, $^{***}P < 0{\cdot}05$ *versus* HV groups.

conditions in the host. In particular, the differences in sex and age between HV and patients with sarcoidosis might affect these results, because we found some HV with a high level of IP-10/CXCL10 in the serum.

There is little information regarding patients with the different stages of sarcoidosis. Capelli *et al.* reported that the highest level of macrophage inflammatory protein (MIP)-1α at stage III and MIP-1β at stage II of sarcoidosis were observed [10]. Shigehara *et al.* reported that IL-18 was high at stages I and II [27]. In the present study, Mig/CXCL9 and IP-10/CXCL10 in BALF were highest at stage II, suggesting that these CXCR3 ligands were involved in the active phase of granulomatous responses in the lungs. Recently, Takeuchi *et al.* reported that serum levels of two CXCR3 ligands, Mig/CXCL9 and IP-10/CXCL10, correlated with disease activity of ocular sarcoidosis [28]. They showed that there was no significant difference in the levels of Mig/CXCL9 and IP-10/CXCL10 between in patients with ocular sarcoidosis with bilateral hilar lymphadenopathy (BHL) and in those without BHL. Considering these findings, our data revealed that the patients with stage II, but not stage I, of pulmonary sarcoidosis showed the elevated levels of serum Mig/CXCL9, suggests that pulmonary infiltrations might be related with the elevation of serum Mig/CXCL9. Further analysis, including ocular sarcoidosis, would be useful to clarify the role of CXCR3 ligands in sarcoidosis.

Alveolar macrophages appeared to be the main producers of CXCR3 ligands in the sarcoid lungs as alveolar macrophages harvested from BAL expressed high levels of CXCR3 ligands, and were stained by immunostaining using the three anti-CXCR3 antibodies. The epithelioid cells and giant cells also appeared to produce these CXCR3 ligands because positive staining of these cells was observed in immunohistochemistry, as in the cases of IL-12, IL-18 [29] and thioredoxin [30]. As these CXCR3 ligands are expressed in other cells, such as endothelial cells [31] and bronchial epithelial cells [32], further studies are required to explore the expression of CXCR3 ligands in sarcoid lungs.

The level of I-TAC/CXCL11 was ~10-fold lower than those of Mig/CXCL9 and IP-10/CXCL10 in both BALF and serum, and 100–1000-fold lower in the supernatants of alveolar macrophages. However, we cannot rule out the possibility that I-TAC/CXCL11 may play a role in the accumulation of Th1 cells in the sarcoid lungs as I-TAC/CXCL11 has ~100-fold higher affinity to CXCR3 and twice-higher chemotactic activity towards stable CXCR3 transfectants when compared with the other CXCR3 ligands [19]. Furthermore, the strongest staining was observed when anti-I-TAC/CXCL11 anti-

body was used for immunostaining. The forward study would be required to clarify this point.

It has been reported that several Th1-related cytokines and chemokines such as IL-12, IFN-γ, macrophage inflammatory protein (MIP)-1α, MIP-1β and CXCL16 were elevated in BALF of patients with sarcoidosis [7,10,29,33]. In the present study, the levels of CXCR3 ligands in BALF were correlated positively with the number of $CD4^+$ lymphocytes. These data suggest that CXCR3 ligands, in addition to other Th1-related factors, act as important chemotactic factors for $CD4^+$ Th1 cells in sarcoid lungs as most $CD4^+$ cells (more than 90%) in BAL cells in patients with sarcoidosis were reported to express CXCR3 [12].

In summary, the results of the present study suggest that Mig/CXCL9 and I-TAC/CXCL11, in addition to IP-10/CXCL10, which are produced from alveolar macrophages, epithelioid and giant cells, play a role in the accumulation of Th1 cells into sarcoid lungs.

Acknowledgements

The authors thank Ms Tomoko Oka for her technical assistance. This work was supported by a grant-in-aid for scientific research by the Ministry of Education, Science, Sports and Culture, Japan.

References

1 American Thoracic Society/European Respiratory Society/World Association of Sarcoidosis and Other Granulomatous Disorders. Statement on sarcoidosis. Am J Respir Crit Care Med 1999; **160**:736–55.

2 Costabel U. Sarcoidosis: clinical update. Eur Respir J 2001; **18**:s56–68.

3 Baughman RP, Lower EE, du Bois R. Sarcoidosis. Lancet 2003; **361**:1111–18.

4 Nunes H, Soler P, Valeyre D. Pulmonary sarcoidosis. Allergy 2005; **60**:565–82.

5 Lopez AF, Sanderson CJ, Gamble JR, Campbell HD, Young IG, Vadas MA. Recombinant human interleukin 5 is a selective activator of human eosinophil function. J Exp Med 1988; **167**:219–24.

6 Wahlstrom J, Katchar K, Wigzell H, Olerup O, Eklund A, Grunewald J. Analysis of intracellular cytokines in $CD4^+$ and $CD8^+$ lung and blood T cells in sarcoidosis. Am J Respir Crit Care Med 2001; **163**:115–21.

7 Prasse A, Georges CG, Biller H *et al.* Th1 cytokine pattern in sarcoidosis is expressed by bronchoalveolar $CD4^+$ and $CD8^+$ T cells. Clin Exp Immunol 2000; **122**:241–8.

8 Bergeron A, Bonay M, Kambouchner M *et al.* Cytokine patterns in tuberculous and sarcoid granulomas: correlation with histopathologic features of the granulomatous response. J Immunol 1997; **159**:3034–43.

9 Bonecchi R, Bianchi G, Bordignon PP *et al.* Differential expression of chemokine receptors and chemotactic responsiveness of type 1 T helper cells (Th1s) and Th2s. J Exp Med 1998; **187**:129–34.

10 Capelli A, di Stefano A, Lusuards M, Gnemmi I, Donner CF. Increased macrophage inflammatory protein-1α and macrophage inflammatory protein-1β levels in bronchoalveolar lavage fluid of patients affected by different stages of pulmonary sarcoidosis. Am J Respir Crit Care Med 2002; **165**:236–41.

11 Agostini C, Cassatella M, Zambello R *et al.* Involvement of the IP-10 chemokine in sarcoid granulomatous reactions. J Immunol 1998; **161**:6413–20.

12 Katchar K, Eklund A, Grunewald J. Expression of Th1 markers by lung accumulated T cells in pulmonary sarcoidosis. J Intern Med 2003; **254**:564–71.

13 Miotto D, Christodoulopoulos P, Olivenstein R *et al.* Expression of IFN-γ-inducible protein; monocyte chemotactic proteins 1, 3, and 4; and eotaxin in T_H1- and T_H2-mediated lung disease. J Allergy Clin Immunol 2001; **107**:664–70.

14 Tani K, Ogushi F, Huang L, Kawano T, Tada H, Hariguchi N, Sone S. CD13/aminopeptidase N, a novel chemoattractant for T lymphocytes in pulmonary sarcoidosis. Am J Respir Crit Care Med 2000; **161**:1636–42.

15 Manabe K, Nishioka Y, Kishi J *et al.* Elevation of macrophage-derived chemokine in eosinophilic pneumonia: a role of alveolar macrophages. J Med Invest 2005; **52**:85–92.

16 Nishioka Y, Yano S, Fujiki F *et al.* Combined therapy of multidrug-resistant human lung cancer with anti-P-glycoprotein antibody and monocyte chemoattractant protein-1 gene transduction: the possibility of immunological overcoming of multidrug resistance. Int J Cancer 1997; **71**:170–7.

17 Farber JM. A macrophage mRNA selectively induced by γ-interferon encodes a member of the platelet factor 4 family of cytokines. Proc Natl Acad Sci USA 1990; **87**:5238–42.

18 Luster AD, Unkeless JC, Ravetch JV. γ-Interferon transcriptionally regulates an early-response gene containing homology to platelet proteins. Nature 1985; **315**:672–6.

19 Cole KE, Strick CA, Paradis TJ *et al.* Interferon-inducible T cell alpha chemoattractant (I-TAC): a novel non-ELR CXC chemokine with potent activity on activated T cells through selective high affinity binding to CXCR3. J Exp Med 1998; **187**:2009–21.

20 Goto H, Yano S, Zhang H *et al.* Activity of a new vascular targeting agent, ZD6126, in pulmonary metastases by human lung adenocarcinoma in nude mice. Cancer Res 2002; **62**:3711–5.

21 Zhao DX-M, Hu Y, Miller GG, Luster AD, Mitchell RN, Libby P. Differential expression of the IFN-γ-inducible CXCR3-binding chemokines, IFN-inducible protein 10, monokine induced by IFN, and IFN-inducible T cell α chemoattractant in human cardiac allografts: association with cardiac allograft vasculopathy and acute rejection. J Immunol 2002; **169**:1556–60.

22 Nishioka Y, Nishimura N, Suzuki Y, Sone S. Human monocyte-derived and $CD83^+$ blood dendritic cells enhance NK cell-mediated cytotoxicity. Eur J Immunol 2001; **31**:2633–41.

23 Hildebrandt GC, Corrion LA, Olkiewicz KM *et al.* Blockade of CXCR3 receptor : ligand interactions reduces leukocyte recruitment to the lung and the severity of experimental idiopathic pneumonia syndrome. J Immunol 2004; **173**:2050–9.

24 Nance S, Cross R, Fitzpatrick E. Chemokine production during hypersensitivity pneumonitis. Eur J Immunol 2004; **34**:677–85.

25 Belperio JA, Keane MP, Burdick MD *et al.* Critical role for CXCR3 chemokine biology in the pathogenesis of bronchiolitis obliterans syndrome. J Immunol 2002; **169**:1037–49.

26 Pignatti P, Brunetti G, Moretto D *et al.* Role of the chemokine receptors CXCR3 and CCR4 in human pulmonary fibrosis. Am J Respir Crit Care Med 2006; **173**:310–7.

27 Shigehara K, Shijubo N, Ohmichi M *et al.* Increased levels of interleukin-18 in patients with pulmonary sarcoidosis. Am J Respir Crit Care Med 2000; **162**:1979–82.

28 Takeuchi M, Oh IK, Suzuki J *et al.* Elevated serum levels of CXCL9/monokine induced by interferon-γ and CXCL10/interferon-γ-inducible protein-10 in ocular sarcoidosis. Invest Ophthalmol Vis Sci 2006; **47**:1063–8.

29 Shigehara K, Shijubo N, Ohmichi M *et al.* IL-12 and IL-18 are increased and stimulate IFN-γ production in sarcoid lungs. J Immunol 2001; **166**:642–9.

30 Koura T, Gon Y, Hashimoto S *et al.* Expression of thioredoxin in granulomas of sarcoidosis: possible role in the development of T lymphocyte activation. Thorax 2000; **55**:755–61.

31 Marx N, Mach F, Sauty A *et al.* Peroxisome proliferator-activated receptor-γ activators inhibit IFN-γ-induced expression of the T cell-active CXC chemokines IP-10, Mig, and I-TAC in human endothelial cells. J Immunol 2000; **164**:6503–8.

32 Sauty A, Dziejman M, Taha RA *et al.* The T cell-specific CXC chemokines IP-10, Mig, and I-TAC are expressed by activated human bronchial epithelial cells. J Immunol 1999; **162**:3549–58.

33 Agostini C, Cabrelle A, Calabrese F *et al.* Role for CXCR6 and its ligand CXCL16 in the pathogenesis of T cell alveolitis in sarcoidosis. Am J Respir Crit Care Med 2005; **172**:1290–8.

Role of α_1-Acid Glycoprotein in Therapeutic Antifibrotic Effects of Imatinib with Macrolides in Mice

Momoyo Azuma[1], Yasuhiko Nishioka[1], Yoshinori Aono[1], Mami Inayama[1], Hideki Makino[1], Jun Kishi[1], Masayuki Shono[2], Katsuhiro Kinoshita[1], Hisanori Uehara[3], Fumitaka Ogushi[4], Keisuke Izumi[3], and Saburo Sone[1]

[1]Department of Internal Medicine and Molecular Therapeutics, [2]Support Center for Advanced Medical Sciences, and [3]Department of Molecular and Environmental Pathology, Institute of Health Biosciences, University of Tokushima Graduate School, Tokushima, Japan; and [4]Clinical Research Center for Allergy and Rheumatology, National Kochi Hospital, Kochi, Japan

Rationale: Imatinib is an inhibitor of platelet-derived growth factor receptors. We have reported that treatment with imatinib inhibited bleomycin-induced pulmonary fibrosis in mice. However, late treatment with imatinib had no effect.

Objectives: To clarify why imatinib had no antifibrotic effect when its administration was delayed, we focused on α_1-acid glycoprotein (AGP), because it was reported to bind imatinib and mediate drug resistance.

Methods: The concentration of AGP in serum of mice and patients with idiopathic pulmonary fibrosis was measured by radial immunodiffusion testing. The effects of AGP *in vitro* were evaluated by assaying the growth of lung fibroblasts. We examined the combined effects of erythromycin (EM) or clarithromycin (CAM) on bleomycin-induced pulmonary fibrosis in mice.

Measurements and Main Results: Addition of AGP abrogated imatinib-mediated inhibition of the growth of fibroblasts. However, treatment with EM or CAM restored the growth-inhibitory effects of imatinib. The elevated level of AGP was detected in serum and lung homogenates in bleomycin-exposed mice and reached a plateau on Day 14. Imatinib alone did not ameliorate pulmonary fibrosis when treatment was started on Day 15, whereas coadministration of imatinib and EM or CAM significantly reduced the fibrogenesis via inhibition of the growth of fibroblasts *in vivo*. Serum levels of AGP were higher in patients with idiopathic pulmonary fibrosis than in healthy subjects.

Conclusions: AGP is an important regulatory factor modulating the ability of imatinib to prevent pulmonary fibrosis in mice, and combined therapy with imatinib and EM or CAM might be useful for treatment of pulmonary fibrosis.

Keywords: platelet-derived growth factor; erythromycin; clarithromycin; fibroblast

Idiopathic pulmonary fibrosis (IPF) is a progressive and lethal disease of the lungs characterized by the proliferation of fibroblasts and deposition of extracellular matrix (1, 2). Although corticosteroids and other immunosuppressants have been used to treat IPF, the 5-year survival rate of patients with the disease is less than 50% (3, 4). For this reason, novel therapeutic modalities are of great interest.

AT A GLANCE COMMENTARY

Scientific Knowledge on the Subject

Imatinib inhibited pulmonary fibrosis using a bleomycin model in mice. However, while early treatment (Days 0 to 15) prevented pulmonary fibrosis, late treatment (Days 15 to 28) did not.

What This Study Adds to the Field

Coadministration of imatinib with macrolides reduced pulmonary fibrosis in mice even if started on Day 15.

Imatinib mesylate (Gleevec in the United States and Glivec in Europe) is a potent and specific tyrosine kinase inhibitor acting against bcr-abl, c-kit, and platelet-derived growth factor receptor (PDGFR) (5). Imatinib has been demonstrated to be highly active against chronic myeloid leukemia and gastrointestinal stromal tumors (6–9). Likewise, in some patients with hypereosinophilic syndrome or myeloproliferative diseases having an activated *PDGFRA* or *PDGFRB* as a fusion gene, imatinib showed marked therapeutic effects, indicating that it could be an clinically useful PDGFR inhibitor (10, 11). Because PDGF is one of the growth factors playing a role in the pathogenesis of pulmonary fibrosis (12, 13), imatinib has the potential to be useful for the treatment of this disease.

Based on these concepts, we and Daniels and colleagues demonstrated that treatment with imatinib inhibited the development of pulmonary fibrosis using a bleomycin model in mice (14, 15). Furthermore, Abdollahi and coworkers demonstrated the antifibrotic effects of imatinib in murine radiation-induced lung fibrosis (16). Imatinib has also been reported to prevent fibrogenesis in the liver and kidneys (17–20). These results suggest that imatinib might serve as an antifibrotic drug for various fibrotic diseases in humans. In fact, a clinical trial of imatinib in patients with IPF is in progress (21).

However, we found that early treatment (from Days 0 to 15) significantly prevented the development of pulmonary fibrosis in the bleomycin model in mice, whereas late treatment (from Days 15 to 28) did not (15). Neef and colleagues also reported that early (from Days 0 to 21), but not late (from Days 22 to 35) treatment was effective in inhibiting liver fibrosis using a bile duct ligation model (20). These results raise the critical question of whether the antifibrotic effects of imatinib are only prophylactic, not therapeutic.

We therefore examined the mechanisms involved in the failure of imatinib to act in the late phase of pulmonary fibrosis in the bleomycin model. First, we hypothesized that there were some mechanisms of resistance to imatinib in late fibrogenesis, and focused on α_1-acid glycoprotein (AGP), which is a major drug binding protein and was reported to

(Received in original form February 2, 2007; accepted in final form August 23, 2007)

Supported by grants from the Ministry of Health and Welfare and the Ministry of Education, Science, Sports, and Culture of Japan.

Correspondence and requests for reprints should be addressed to Yasuhiko Nishioka, M.D., Ph.D., Department of Internal Medicine and Molecular Therapeutics, Institute of Health Biosciences, University of Tokushima Graduate School, 3-18-15 Kuramoto-cho, Tokushima 770-8503, Japan. E-mail: yasuhiko@clin.med.tokushima-u.ac.jp

This article has an online supplement, which is accessible from this issue's table of contents at www.atsjournals.org

Am J Respir Crit Care Med Vol 176. pp 1243–1250, 2007
Originally Published in Press as DOI: 10.1164/rccm.200702-178OC on August 23, 2007
Internet address: www.atsjournals.org

bind imatinib and mediate drug resistance (22, 23). We also examined the effects of 14-membered ring macrolides, including erythromycin (EM) and clarithromycin (CAM), which can compete with imatinib to bind AGP, on the AGP-mediated suppression of imatinib's actions *in vitro* and *in vivo*. Some of the results of these studies have been reported previously in the form of an abstract (24).

METHODS

Detailed methods are described in the online supplement.

Mice and Materials

Eight-week-old female C57BL/6 mice were purchased from Charles River Japan, Inc. (Yokohama, Japan). They were maintained in the animal facility of the University of Tokushima under specific pathogen–free conditions according to the guidelines of our university (15, 25). Imatinib mesylate was kindly provided by Dr. Elisabeth Buchdunger (Novartis, Basel, Switzerland). EM, bovine serum albumin, AGP, and PDGF-BB were purchased from Sigma-Aldrich (St. Louis, MO). CAM was obtained from Wako Pure Chemical Industries, Ltd. (Osaka, Japan). Bleomycin was purchased from Nippon Kayaku Co. (Tokyo, Japan).

Bleomycin Treatment

Osmotic minipumps (model 2001; Alza Pharmaceuticals, Palo Alto, CA) containing 200 μl of saline with or without bleomycin (125 mg/kg) were implanted subcutaneously (15, 26, 27). Each experiment was performed in at least three mice per group.

Administration of Imatinib, EM, and CAM

Imatinib powder was dissolved in distilled water (Otsuka Pharmaceutical Co., Tokushima, Japan). EM and CAM were first dissolved in ethanol and then diluted in distilled water. Imatinib (50 mg/kg/d) was injected intraperitoneally, and EM (5 mg/kg/d) or CAM (20 mg/kg/d) was administered subcutaneously from Days 15 to 28 (15).

Collagen Assay

The right lungs were harvested on Day 28. The total amount of collagen in the lungs was determined using the Sircol Collagen Assay kit (Biocolor Ltd., Belfast, Northern Ireland) (15, 27).

Histopathology

The left lungs were fixed in 10% buffered formalin and embedded in paraffin. Sections (3 to 4 μm) were stained with hematoxylin and eosin. For quantitative histologic analysis, a numerical fibrotic scale was used (Ashcroft score) (28). The mean score was considered the fibrotic score. Masson's trichrome staining was also performed.

Fibroblast Isolation

Murine lung fibroblasts were generated according to the method reported by Phan and coworkers (29). These fibroblasts were used at 5 to 10 passages.

Proliferation Assay

Cell proliferation was evaluated by assaying incorporation of ^{3}H-thymidine deoxyribose (TdR) (19). The experiments were performed in triplicate.

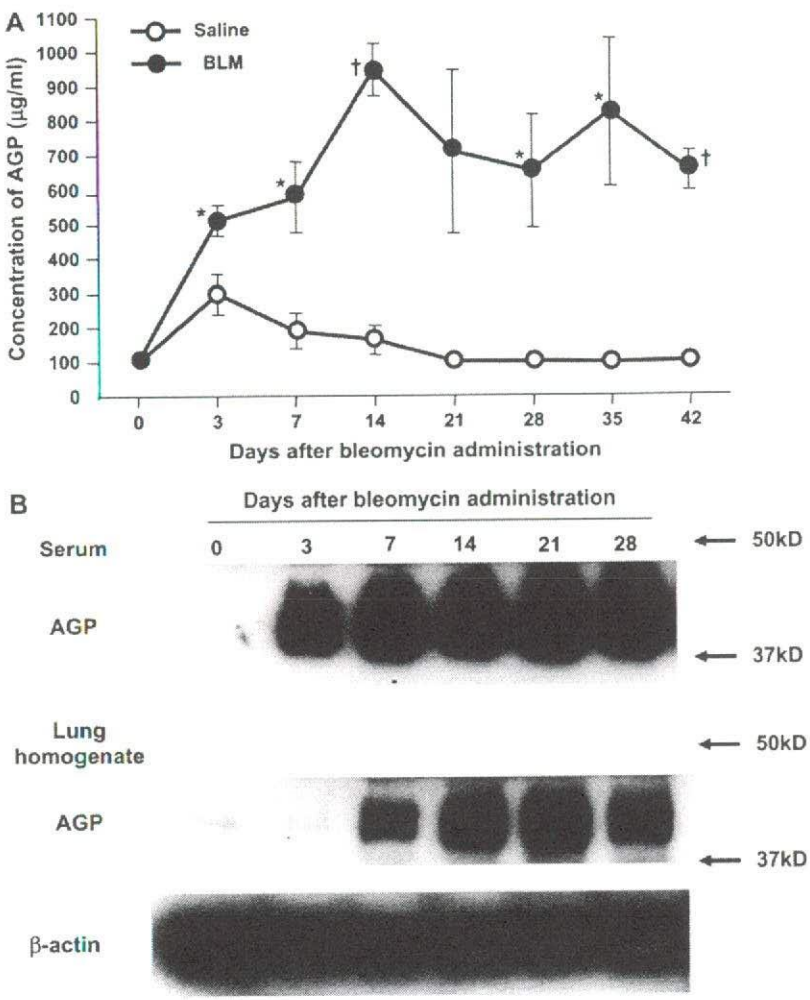

Figure 1. The levels of α_1-acid glycoprotein (AGP) in serum and lung homogenates are elevated in bleomycin-treated mice. Mice were implanted with osmotic minipumps containing saline or bleomycin (125 mg/kg). On the days indicated, three mice per group were killed after blood was harvested from the axillary artery. (*A*) Elevated level of AGP in serum of mice treated with bleomycin. The level of AGP was determined by radial immunodiffusion assay. Data are presented as the mean ± SD of three mice. Similar results were obtained in two separate experiments. $^*P < 0.001$ versus group treated with saline; $^\dagger P < 0.05$ versus group treated with saline. (*B*) Immunoblot analysis for murine AGP. Immunoblotting for AGP with murine serum (1 μl) and lung homogenates (50 μg) was performed as described in the online supplement. Data are representative of three experiments with the different samples from three mice. BLM = bleomycin.

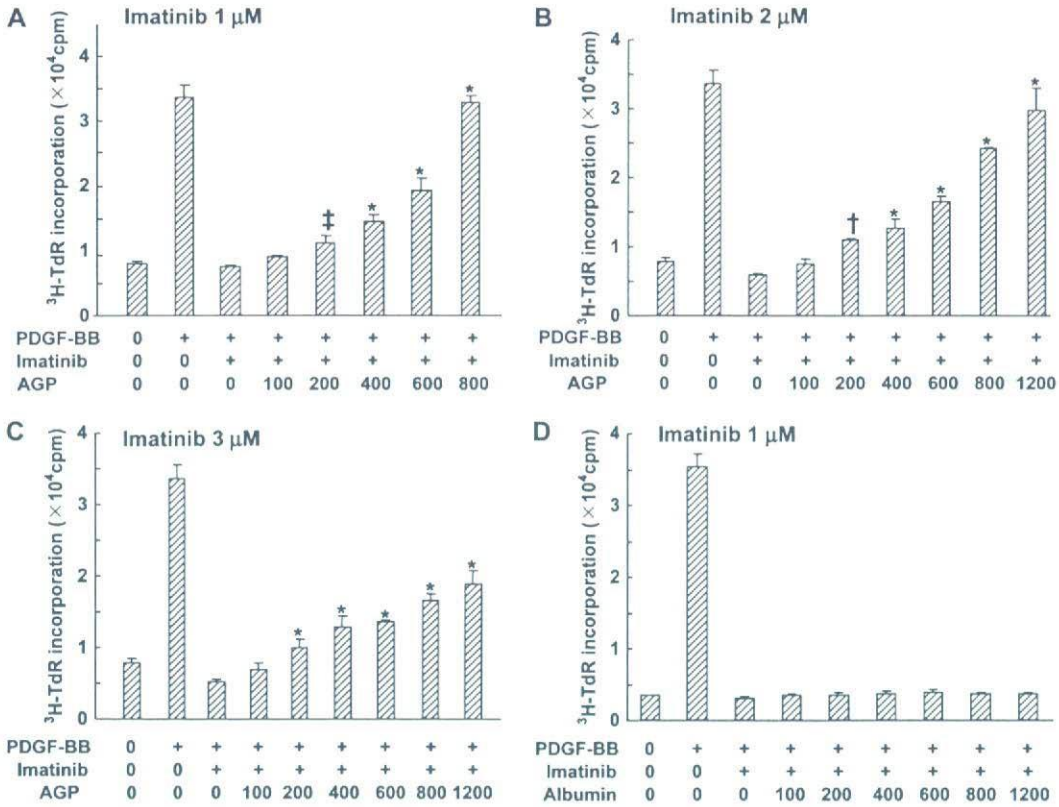

Figure 2. α_1-Acid glycoprotein (AGP) abrogates the inhibitory effects of imatinib on PDGF-BB–stimulated DNA synthesis in lung fibroblasts. Primary lung fibroblasts (8×10^3 cells/well) were stimulated with PDGF-BB (10 ng/ml). Addition of imatinib (1–3 μM) significantly inhibited the proliferation of lung fibroblasts stimulated with PDGF-BB. AGP (*A–C*) or albumin (*D*) was added at various doses (0–1,200 μg/ml). Cells were labeled with ^{3}H-thymidine deoxyribose (^{3}H-TdR) at 1 μCi/well for the final 18 hours and the incorporation of ^{3}H-TdR was measured with a liquid scintillation counter. Data are presented as the mean ± SD of triplicate cultures. Similar results were obtained in three separate experiments. $^*P < 0.001$; $^\dagger P < 0.01$; or $^\ddagger P < 0.05$ versus group treated with PDGF-BB and imatinib.

Determination of the Concentration of AGP

The concentration of AGP was measured in murine and human serum. The assay was performed using a single radial immunodiffusion plate test (Cardiotech Services, Inc., Louisville, KY) (22). The human study was approved by the ethics committee of the University of Tokushima, and written, informed consent was obtained from all the subjects. IPF was diagnosed according to the American Thoracic Society international consensus statement (3).

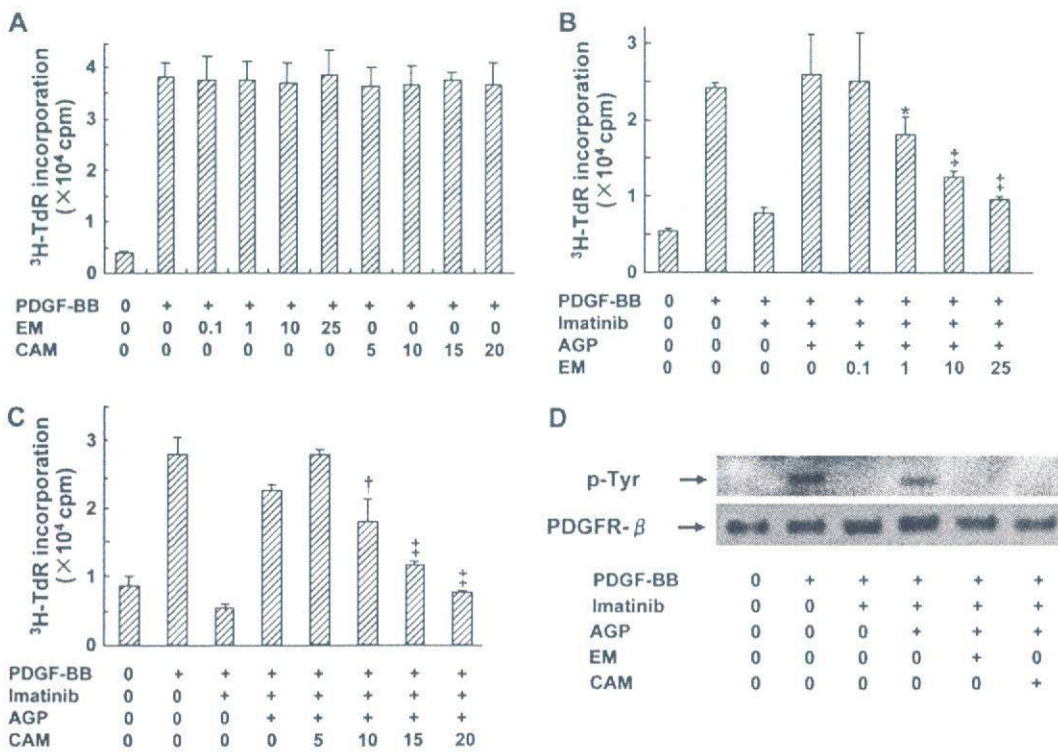

Figure 3. Addition of erythromycin (EM) or clarithromycin (CAM) reverses α_1-acid glycoprotein (AGP)–mediated suppression and restores the biological activity of imatinib *in vitro*. Primary lung fibroblasts were cultured with PDGF-BB (10 ng/ml), imatinib (1 μM), and AGP (800 μg/ml). EM (*A, B*) or CAM (*A, C*) was added at various doses (0–25 μM) as indicated. Data are representative of three separate experiments. Cells were pulsed with ^{3}H-thymidine deoxyribose (^{3}H-TdR) (1 μCi/well) for the final 18 hours and the incorporation of ^{3}H-TdR was measured with a liquid scintillation counter. Data are presented as the mean ± SD of triplicate cultures. Similar results were obtained in three separate experiments. $^*P < 0.001$; $^\dagger P < 0.01$; or $^\ddagger P < 0.05$ versus the group treated with PDGF-BB, imatinib, and AGP. (*D*) Immunoblot analysis for tyrosine phosphorylation of PDGFR in primary lung fibroblasts. Primary lung fibroblasts were stimulated with PDGF-BB (10 ng/ml) for 10 minutes. Cell lysates were separated on a 7.5% sodium dodecyl sulfate–polyacrylamide gel electrophoresis and transferred to a nitrocellulose membrane. Immunoblotting was performed with the indicated antibodies. Data are representative of three separate experiments.

Immunoblotting

Immunoblotting for PDGFR and AGP was performed as described previously (15).

Immunostaining

Paraffin-embedded lung sections were stained with rat anti-mouse Ki-67 antigen antibody (Dako, Glostrup, Denmark) using a ready-to-use Vectastain Quick Kit (Vector Laboratories, Burlingame, CA) (15).

Immunofluorescent double-staining was performed with anti-mouse Ki-67 and anti-S100A4/FSP1 antibodies (Lab Vision Corp., Fremont, CA). Fluorescence images were analyzed using a confocal laser scanning microscope (TCS NT; Leica, Heidelberg, Germany) (30).

Statistical Analysis

Comparisons among multiple groups were performed using one-way analysis of variance with Newman-Keuls post hoc correction (GraphPad Prism, version 3.0; GraphPad, San Diego, CA). Correlation coefficients were determined using Pearson's linear regression analysis. The statistical analysis was performed with StatView software (SAS Institute, Inc., Cary NC). Differences were considered statistically significant if P values were less than 0.05.

RESULTS

The Level of AGP in Serum and Lung Homogenates Is Elevated in Bleomycin-treated Mice

We first examined serum levels of AGP in mice after the administration of bleomycin. The results are shown in Figure 1A. Levels in untreated mice were 90 to 110 μg/ml. After the administration of bleomycin, AGP levels were increased rapidly from Day 3, reaching a plateau of 650 to 1,000 μg/ml on Day 14. They remained high until Day 42. The transient increase in control mice on Day 3 was considered to be due to the procedure of implantation of osmotic minipumps. The elevated level of AGP in serum of mice was confirmed by Western blotting (Figure 1B).

On the other hand, the expression of AGP in the lungs was also enhanced in bleomycin-exposed mice from Day 7, and reached a plateau on Day 14 (Figure 1B).

AGP Abrogates the Inhibitory Effects of Imatinib on DNA Synthesis of Lung Fibroblasts in Response to PDGF-BB

Next, we examined whether a high concentration of AGP, comparable to the level in serum of bleomycin-treated mice, affects the biological activities of imatinib in an *in vitro* assay. As shown in Figure 2, addition of imatinib significantly inhibited the proliferative responses of lung fibroblasts stimulated with PDGF-BB. Furthermore, addition of AGP abrogated the growth-inhibitory effects of imatinib in a dose-dependent manner (Figures 2A–2C). The reversing effects of AGP were dependent on the concentration of imatinib, and at a concentration of more than 200 μg/ml, AGP significantly inhibited the effects of 1 to 3 μM imatinib (Figures 2A–2C). On the other hand, albumin did not affect the growth-inhibitory effects of imatinib (Figure 2D).

Addition of EM or CAM Reverses AGP- mediated Suppression and Restores the Biological Activity of Imatinib *In Vitro*

Fourteen-membered ring macrolides, including EM and CAM, are known to compete with imatinib to bind AGP (22, 31). Next, we examined whether EM or CAM could reverse the effects of AGP and restore the biological activity of imatinib in an assay of the growth of lung fibroblasts. As shown in Figures 3B and 3C, the addition of either EM or CAM to the culture with AGP (800 μg/ml) and imatinib (1 μM) significantly restored the inhibitory effect of imatinib on the proliferation of lung fibroblasts in a dose-dependent manner. Similar effects of EM or CAM were observed in various doses of AGP (Figure E1 in the online supplement). However, EM or CAM alone did not directly inhibit the uptake of ^{3}H-TdR by fibroblasts stimulated with PDGF-BB (Figure 3A).

To clarify the mechanisms involved in the effects of EM or CAM on AGP-mediated suppression of the growth-inhibitory effects of imatinib, we performed immunoblot analysis for tyrosine phosphorylation of PDGFR. As shown in Figure 3D, imatinib inhibited the autophosphorylation of PDGFR induced by PDGF-BB, and addition of AGP restored PDGF-mediated activation of PDGFR. However, treatment with EM or CAM in

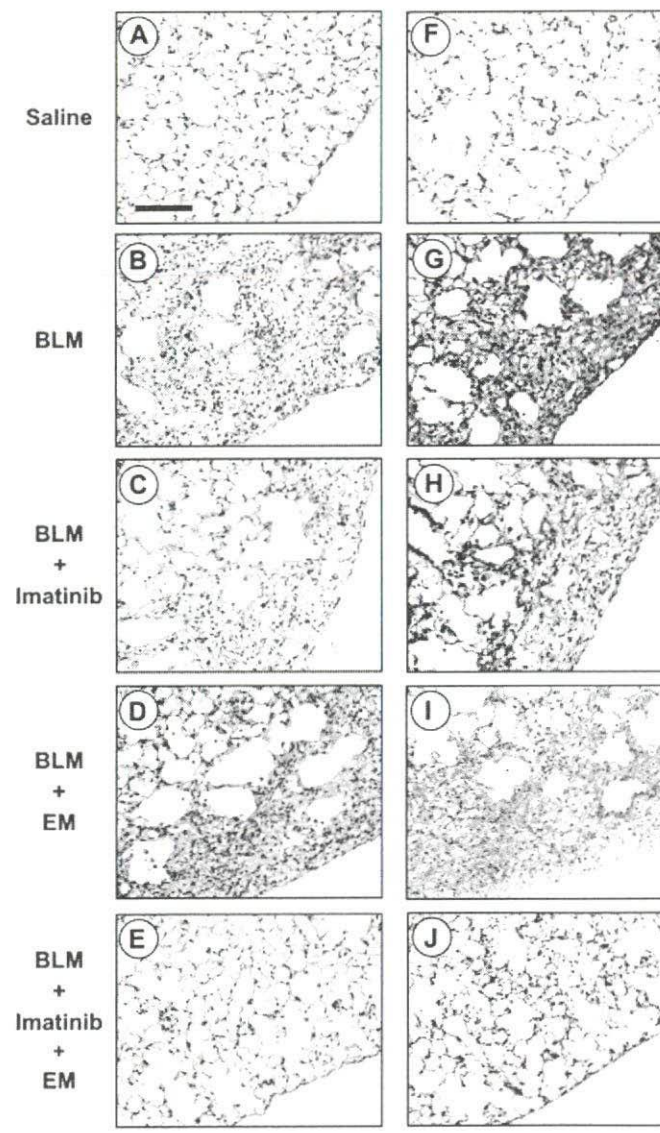

Figure 4. Histologic examination of the antifibrotic effects of the combined use of erythromycin (EM) and imatinib on bleomycin (BLM)-induced pulmonary fibrosis. Mice were implanted with osmotic minipumps containing BLM. Imatinib (50 mg/kg/d) and/or EM (5 mg/kg/d) was intraperitoneally injected from Days 15 to 28. On Day 28, mice were killed and histologic examination was performed using hematoxylin-and-eosin staining (*A, C, E, G, I*) and Masson's trichrome staining (*B, D, F, H, J*) (original magnification, ×200). (*A, F*) Phosphate-buffered saline; (*B, G*) BLM alone; (*C, H*) BLM + imatinib; (*D, I*) BLM + EM; (*E, J*) BLM + imatinib + EM. Data are representative of three separate experiments. *Bar* = 100 μm.

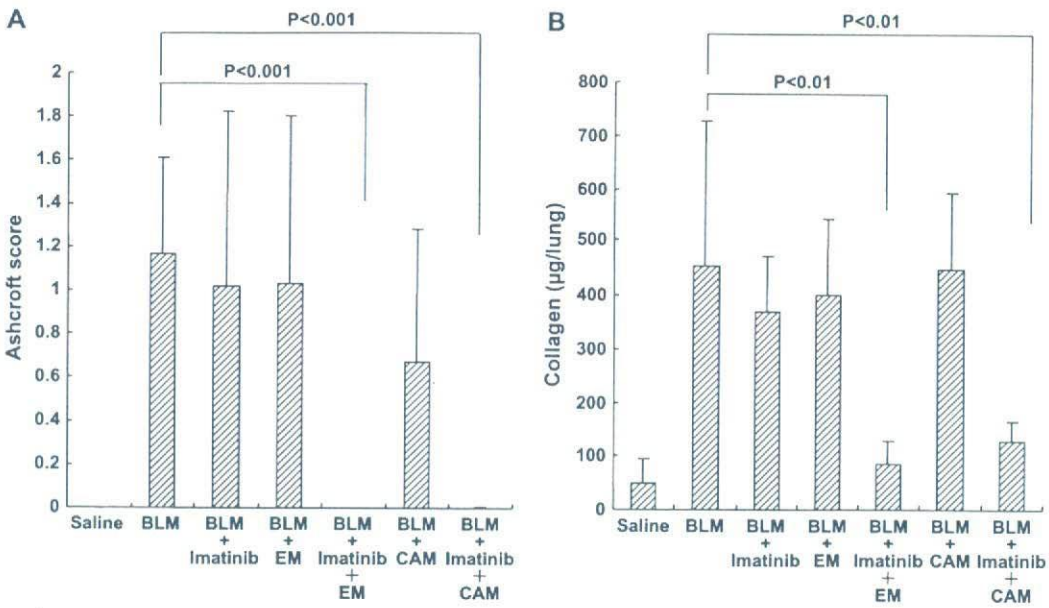

Figure 5. Quantitative examinations of therapeutic antifibrotic effects of imatinib and macrolide antibiotics on bleomycin (BLM)-induced pulmonary fibrosis. Mice were implanted with osmotic minipumps containing saline or BLM. Imatinib (50 mg/kg/d), erythromycin (EM) (5 mg/kg/d), or clarithromycin (CAM) (20 mg/kg/d) was intraperitoneally injected from Days 15 to 28. Mice were killed on Day 28. (*A*) Evaluation of fibrotic change in the lung using a numerical fibrotic score. The histologic examination of the left lung was performed with hematoxylin-and-eosin staining. The fibrotic score was determined by two pathologists as described in METHODS. Data are presented as the mean ± SD of all fields examined in each group of five mice. (*B*) Effects of imatinib on the deposition of collagen after treatment with BLM. The amount of collagen in the right lung was measured using a Sircol collagen kit. Data are presented as the mean ± SD in each group of five mice. Data are representative of three separate experiments.

the presence of AGP and imatinib inhibited the tyrosine phosphorylation of PDGFR, indicating the restoration of the function of imatinib.

Combination of EM or CAM with Imatinib Exerts "Therapeutic" Antifibrotic Effects in Bleomycin-induced Pulmonary Fibrosis in Mice

We further examined the *in vivo* antifibrotic effects of combined therapy with imatinib and EM or CAM using a bleomycin-induced model of fibrosis in the lungs. In this experiment, bleomycin-treated mice were injected with imatinib and/or EM or CAM from Days 14 to 28 (late treatment). Consistent with previous reports (15, 32), neither imatinib nor the macrolides alone showed any antifibrotic effects with this treatment schedule (Figures 4 and 5). However, combined therapy with imatinib and EM or CAM resulted in a significant reduction in the number of fibrotic lesions in subpleural areas of the lung even when both agents were administered from Days 14 to 28 (late treatment) (Figures 4 and 5). Quantitative histologic analysis demonstrated that the fibrotic score was significantly lower in mice treated with imatinib and EM or CAM than those treated with bleomycin alone (bleomycin, 1.18 ± 0.08, vs. bleomycin + imatinib + EM, 0 ± 0; $P < 0.001$; bleomycin + imatinib + CAM, 0 ± 0; $P < 0.001$) (Figure 5A). The amount of collagen in the lung was also significantly smaller in mice treated with imatinib and EM or CAM as opposed to bleomycin alone (bleomycin, 456 ± 272, vs. bleomycin + imatinib + EM, 87 ± 41; $P < 0.01$; bleomycin + imatinib + CAM, 128 ± 37 μg/ml; $P < 0.01$) (Figure 5B).

Inhibition of Mitogenesis of Pulmonary Fibroblasts by Treatment with Imatinib plus Macrolide in Bleomycin-induced Lung Fibrosis *In Vivo*

To analyze the mechanism by which combined therapy with imatinib and macrolide attenuated bleomycin-induced lung fibrosis when the treatment was started on Day 14, we examined whether imatinib plus macrolide inhibited the proliferation of lung fibroblasts *in vivo* on Day 21. Proliferating cells, which were stained with anti–Ki-67 antigen antibody, were detected in the fibrotic areas of bleomycin-treated lungs (Figures 6B–6E). We found a few Ki-67–positive cells in the alveolar wall (Figure 6A), but there was no difference in the number of these cells among the treatment groups (Figure 6F). On the other hand, the proliferating mesenchymal cells in the interalveolar space of the lungs were significantly reduced in mice treated with both imatinib and EM compared with the other groups (Figure 6F).

Furthermore, to confirm that the proliferating mesenchymal cells were fibroblasts, we performed immunofluorescent double-staining for a fibroblast-specific marker, S100A4/FSP1, and Ki-67 antigen. The confocal microscopic analysis clearly showed that most Ki-67–positive cells were also positive for S100A4/FSP1 staining (Figure 7).

Serum Levels of AGP in Patients with IPF

Finally, we measured the levels of AGP in patients with IPF to examine whether AGP-mediated inhibition of the biological activity of imatinib occurs in humans. Serum AGP levels were significantly higher in patients with IPF than in healthy volunteers (1056 ± 555 vs. 455 ± 165 μg/ml, $P < 0.001$) (Figure 8A). The concentration of AGP was not correlated with that of C-reactive protein (Figure 8B).

DISCUSSION

In the present study, we demonstrated that AGP plays a pivotal role in the antifibrotic effects of imatinib both *in vitro* and *in vivo*, and that the coadministration of 14-membered ring macrolides was effective for producing therapeutic, not prophylactic, effects of imatinib in bleomycin-induced pulmonary fibrosis in mice. Furthermore, because the level of AGP was elevated in the serum of patients with IPF, a similar therapeutic effect of such combined treatment might also be predicted in humans.

We and Daniels and colleagues have previously reported that imatinib prevented the development of pulmonary fibrosis in mice using bleomycin- and radiation-induced models (14, 15). However, when the time course of the antifibrotic effects was

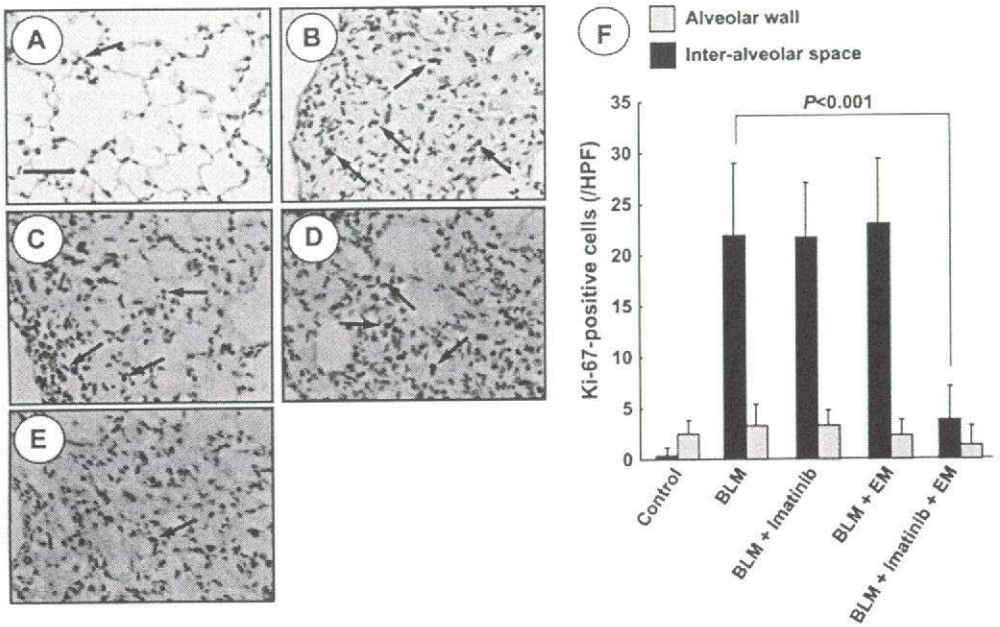

Figure 6. Coadministration of imatinib and erythromycin (EM) reduces the proliferating mesenchymal cells in the lungs of mice treated with bleomycin (BLM). Mice were implanted with osmotic minipumps containing BLM. Imatinib (50 mg/kg/d) and/or EM (5 mg/kg/d) was administered from Days 15 to 21. On Day 21, mice were killed and immunohistochemical analysis using anti–Ki-67 antigen antibody was performed. (*A*) Phosphate-buffered saline; (*B*) BLM alone; (*C*) BLM + imatinib; (*D*) BLM + EM; (*E*) BLM + imatinib + EM (original magnification, ×400). *Bar* = 50 μm; *arrows* = Ki-67–positive nuclei. (*F*) Quantitative analysis of Ki-67–positive cells. The Ki-67–positive cells in 20 random fields were counted at ×400 original magnification. Data represent three separate experiments, means ± SD.

examined, late treatment with imatinib was found not to be effective in inhibiting pulmonary fibrosis (15), indicating that imatinib might have only a prophylactic, not a therapeutic, effect. These characteristics are of great importance if imatinib is to be used clinically. We therefore examined whether it is more likely that mechanisms of resistance to imatinib exist in the late phase of pulmonary fibrosis, or that imatinib simply does not have therapeutic antifibrotic effects. The present study clearly demonstrated that resistance to imatinib occurred in pulmonary fibrosis, caused by a factor that was identified as AGP. More than 400 μg/ml of AGP significantly reduced the imatinib-mediated suppression of the growth of lung fibroblasts *in vitro*. In addition, from 700 to 1,000 μg/ml of AGP was detected in the serum of bleomycin-treated mice, indicating the relevance *in vivo* of the AGP-mediated suppression of imatinib in mice.

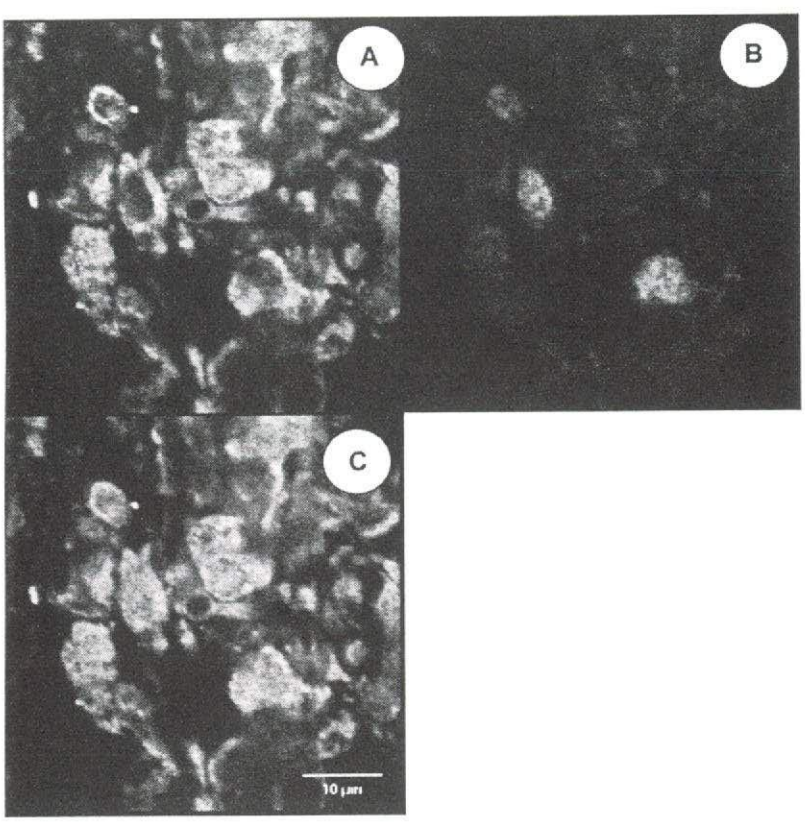

Figure 7. Confocal immunofluorescence microscope images of tissue slices of the lungs of bleomycin-treated mice with staining for S100A4/FSP1 and Ki-67 antigen. Mice were implanted with osmotic minipumps containing bleomycin. On Day 21, mice were killed and paraffin-embedded lung sections were stained with rat anti–Ki-67 antigen monoclonal antibody (*red*) and rabbit anti-S100A4/FSP1 polyclonal antibody (*green*) (*A*) S100A4/FSP1; (*B*) Ki-67; (C) S100A4/FSP1 + Ki-67. *Bar* = 10 μm.

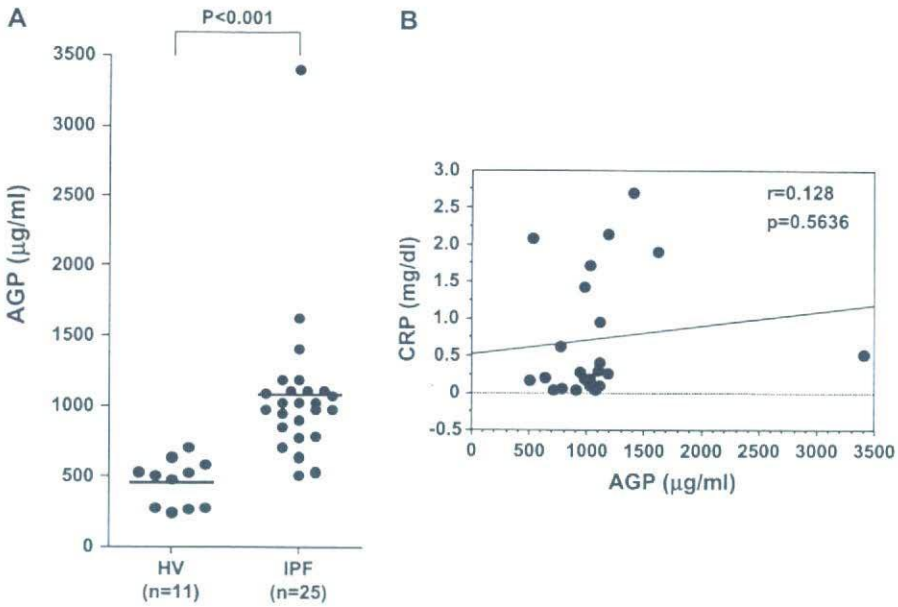

Figure 8. Elevated α_1-acid glycoprotein (AGP) concentrations in patients with idiopathic pulmonary fibrosis (IPF). (*A*) The level of AGP in serum was measured in healthy volunteers (HV) (n = 11) and patients with IPF (n = 25). (*B*) The correlation between the levels of AGP and C-reactive protein (CRP) in serum was examined.

Human serum albumin, lipoprotein, and AGP are the most important drug-binding proteins in plasma (33), and AGP might play a major role in binding imatinib because albumin did not affect imatinib-mediated antiproliferative effects *in vitro*. Next, we examined whether imatinib was likely to have therapeutic antifibrotic effects if the AGP-mediated inhibition was released. To do this, we used 14-membered macrolides, EM and CAM, that compete with imatinib to bind AGP (23). First, the addition of EM or CAM to the culture of lung fibroblasts containing imatinib and AGP clearly reversed the suppressive influence of AGP on the growth-inhibitory effects of imatinib. To abrogate the effects of 800 μg/ml of AGP, more than 1 μM EM or 10 μM CAM was required *in vitro*. Such concentrations are achievable in mice and humans using standard doses of these macrolides (34, 35). Furthermore, we demonstrated that combined use of EM or CAM and imatinib attenuated the bleomycin-induced pulmonary fibrosis in mice partly via inhibiting the growth of fibroblasts even when both agents were administered from Days 14. It was reported that 14-membered macrolides had antifibrotic effects in a bleomycin-induced model when mice were pretreated, but not post-treated, with the drugs (32, 36). These results strongly suggest that the therapeutic antifibrotic effects of imatinib plus EM or CAM were mainly mediated by the restoration of the activity of imatinib by those macrolides. Although the lack of the data regarding the concentration of imatinib in serum and lung tissues could be a limitation of the present study, a pharmacokinetics study by Gambacorti-Passerini and colleagues showed that the coadministration of imatinib with clindamycin increased the tissue distribution of imatinib, and the free imatinib levels in plasma rose slightly (23). However, we could not completely rule out the possibility that other mechanisms, including antiinflammatory effects, of macrolides play a role in these activities (37).

Finally, we demonstrated that the levels of AGP were higher in patients with IPF than in healthy subjects. The concentration of AGP in 12 of 25 patients with IPF (48%) was higher than 1,000 μg/ml, a level that was demonstrated to reverse the antifibrotic effects of imatinib *in vitro*. In our study, substantial differences were found in the baseline levels of AGP between mice and humans (<100 μg/ml vs. 400–800 μg/dl) as described previously (22). However, the plasma concentration of imatinib is also higher in humans than in mice (22). Because the effects of imatinib appear to depend on the balance of the concentrations of imatinib and AGP (as shown in Figures 2A–2C), resistance to imatinib caused by AGP might occur in patients with IPF. To clarify these points, the results of ongoing clinical trial might be helpful and further studies examining the changes of AGP levels in different stages and during disease progression in patients with IPF will be needed.

The reason why AGP levels are high in patients with IPF remains unclear. Because AGP is an acute-phase protein synthesized in the liver, it is reasonable that its levels are elevated in patients with inflammatory diseases (33). However, there was no correlation between the levels of AGP and C-reactive protein in patients with IPF at first diagnosis. Furthermore, the expression of AGP in lung homogenates was enhanced in the late-phase fibrosis. Although the precise biological roles of AGP in pulmonary fibrosis have not been fully determined (33), our data together with the previous findings reporting that alveolar macrophages and type II alveolar epithelial cells in fibrotic lungs were able to produce AGP (38–40) may suggest that AGP was preferentially produced in the fibrotic lungs. Further study will be required to clarify the role of AGP in pulmonary fibrosis.

In summary, the present results suggest that combined therapy with imatinib and macrolides or other drugs that compete with imatinib to bind AGP might be useful for treating pulmonary fibrosis, including IPF.

Conflict of Interest Statement: None of the authors has a financial relationship with a commercial entity that has an interest in the subject of this manuscript.

Acknowledgment: The authors thank Ms. Tomoko Oka for technical assistance.

References

1. Gross TJ, Hunninghake GW. Idiopathic pulmonary fibrosis. *N Engl J Med* 2001;345:517–525.
2. Selman M, King TE Jr, Pardo A. Idiopathic pulmonary fibrosis: prevailing and evolving hypotheses about its pathogenesis and implications for therapy. *Ann Intern Med* 2001;134:136–151.
3. American Thoracic Society. Idiopathic pulmonary fibrosis: diagnosis and treatment [international consensus statement]. *Am J Respir Crit Care Med* 2000;161:646–664.
4. Collard HR, King TE Jr. Demystifying idiopathic interstitial pneumonia. *Arch Intern Med* 2003;163:17–29.
5. Druker BJ, Tamura S, Buchdunger E, Ohno S, Segal GM, Fanning S, Zimmermann J, Lydon NB. Effects of a selective inhibitor of the abl

tyrosine kinase on the growth of bcr-abl positive cells. *Nat Med* 1996;2: 561–566.
6. Druker BJ, Talpaz M, Resta DJ, Peng B, Buchdunger E, Ford JM, Lydon NB, Kantarjian H, Capdeville R, Ohno-Jones S, *et al.* Efficacy and safety of a specific inhibitor of the BCR-ABL tyrosine kinase in chronic myeloid leukemia. *N Engl J Med* 2001;344:1031–1037.
7. Druker BJ, Sawyers CL, Kantarjian H, Resta DJ, Reese SF, Ford JM, Capdeville R, Talpaz M. Activity of a specific inhibitor of the BCR-ABL tyrosine kinase in the blast crisis of chronic myeloid leukemia and acute lymphoblastic leukemia with the Philadelphia chromosome. *N Engl J Med* 2001;344:1038–1042.
8. Demetri GD, von Mehren M, Blanke CD, Van den Abbeele AD, Eisenberg B, Roberts PJ, Heinrich MC, Tuveson DA, Singer S, Janicek M, *et al.* Efficacy and safety of imatinib mesylate in advanced gastrointestinal stromal tumors. *N Engl J Med* 2002;347:472–480.
9. van Oosterom AT, Judson I, Verweij J, Stroobants S, Donato di Paola E, Dimitrijevic S, Martens M, Webb A, Sciot R, Van Glabbeke M, *et al.*; European Organization for Research and Treatment of Cancer Soft Tissue and Bone Sarcoma Group. Safety and efficacy of imatinib (STI571) in metastatic gastrointestinal stromal tumours: a phase I study. *Lancet* 2001;358:1421–1423.
10. Apperley JF, Gardembas M, Melo JV, Russell-Jones R, Bain BJ, Baxter EJ, Chase A, Chessells JM, Colombat M, Dearden CE, *et al.* Response to imatinib mesylate in patients with chronic myeloproliferative diseases with rearrangements of the platelet-derived growth factor receptor beta. *N Engl J Med* 2002;347:481–487.
11. Cools J, DeAngelo DJ, Gotlib J, Stover EH, Legare RD, Cortes J, Kutok J, Clark J, Galinsky I, Griffin JD, *et al.* A tyrosine kinase created by fusion of the PDGFRA and FIP1L1 genes as a therapeutic target of imatinib in idiopathic hypereosinophilic syndrome. *N Engl J Med* 2003;348:1201–1214.
12. Heldin CH, Westermark B. Mechanism of action and in vivo role of platelet-derived growth factor. *Physiol Rev* 1999;79:1283–1316.
13. Li X, Eriksson U. Novel PDGF family members: PDGF-C and PDGF-D. *Cytokine Growth Factor Rev* 2003;14:91–98.
14. Daniels CE, Wilkes MC, Edens M, Kottom TJ, Murphy SJ, Limper AH, Leof EB. Imatinib mesylate inhibits the profibrogenic activity of TGF-β and prevents bleomycin-mediated lung fibrosis. *J Clin Invest* 2004;114:1308–1316.
15. Aono Y, Nishioka Y, Inayama Y, Ugai M, Kishi J, Uehara H, Izumi K, Sone S. Imatinib as a novel antifibrotic agent in bleomycin-induced pulmonary fibrosis in mice. *Am J Respir Crit Care Med* 2005;171: 1279–1285.
16. Abdollahi A, Li M, Ping G, Plathow C, Domhan S, Kiessling F, Lee LB, McMahon G, Grone H-J, Lipson KE, *et al.* Inhibition of platelet-derived growth factor signaling attenuates pulmonary fibrosis. *J Exp Med* 2005;201:925–935.
17. Gilbert RE, Kelly DJ, McKay T, Chadban S, Hill PA, Cooper ME, Atkins RC, Nikolic-Paterson DJ. PDGF signal transduction inhibition ameliorates experimental mesangial proliferative glomerulonephritis. *Kidney Int* 2001;59:1324–1332.
18. Wang S, Wilkes MC, Leof EB, Hirschberg R. Imatinib mesylate blocks a non-Smad TGF-β pathway and reduces renal fibrogenesis in vivo. *FASEB J* 2005;19:1–11.
19. Yoshiji H, Noguchi R, Kuriyama S, Ikenaka Y, Yoshii J, Yanase K, Namisaki T, Kitade M, Masaki T, Fukui H. Imatinib mesylate (STI-571) attenuates liver fibrosis development in rats. *Am J Physiol Gastrointest Liver Physiol* 2005;288:G907–G913.
20. Neef M, Ledermann M, Saegesser H, Schneider V, Widmer N, Decosterd LA, Rochat B, Reichen J. Oral imatinib treatment reduces early fibrogenesis but does not prevent progression in the long term. *J Hepatol* 2006;44:167–175.
21. Bouros D, Antoniou KM. Current and future therapeutic approaches in idiopathic pulmonary fibrosis. *Eur Respir J* 2005;26:693–702.
22. Gambacorti-Passerini C, Barni R, le Coutre P, Zucchetti M, Cabrita G, Cleris L, Rossi F, Gianazza E, Brueggen J, Cozens R, *et al.* Role of α1 acid glycoprotein in the *in vivo* resistance of human BCR-ABL$^+$ leukemic cells to the abl inhibitor STI571. *J Natl Cancer Inst* 2000;92: 1641–1650.
23. Gambacorti-Passerini C, Zucchetti M, Russo D, Frapolli R, Verga M, Bungaro S, Tornaghi L, Rossi F, Pioltelli P, Pogliani E, *et al.* α_1 Acid glycoprotein binds to imatinib (STI571) and substantially alters its pharmacokinetics in chronic myeloid leukemia patients. *Clin Cancer Res* 2003;9:625–632.
24. Azuma M, Nishioka Y, Aono Y, Inayama M, Makino H, Uehara H, Izumi K, Sone S. Inhibition of bleomycin-induced pulmonary fibrosis in mice by imatinib (Gleevec) and erythromycin: a role of α_1-acid glycoprotein [abstract]. *Am J Respir Crit Care Med* 2005;2:A636.
25. Nishioka Y, Yano S, Fujiki F, Mukaida N, Matsushima K, Tsuruo T, Sone S. Combined therapy of multidrug-resistant human lung cancer with anti-P-glycoprotein antibody and monocyte chemoattractant protein-1 gene transduction:the possibility of immunological overcoming of multidrug resistance. *Int J Cancer* 1997;71:170–177.
26. Harrison JH, Lazo JS. High dose continuous infusion of bleomycin in mice: a new model for drug-induced pulmonary fibrosis. *J Pharmacol Exp Ther* 1987;243:1185–1194.
27. Inayama M, Nishioka Y, Azuma M, Muto S, Aono Y, Makino H, Tani K, Uehara H, Izumi K, Itai A, *et al.* A novel IκB kinase-β inhibitor ameliorates bleomycin-induced pulmonary fibrosis in mice. *Am J Respir Crit Care Med* 2006;173:1016–1022.
28. Ashcroft T, Simpson JM, Timbrell V. Simple method of estimating severity of pulmonary fibrosis on a numerical scale. *J Clin Pathol* 1988; 41:467–470.
29. Phan SH, Varani J, Smith D. Rat lung fibroblast collagen metabolism in bleomycin-induced pulmonary fibrosis. *J Clin Invest* 1985;76:241–247.
30. Ishikawa Y, Yuan Z, Inoue N, Skowronski MT, Nakae Y, Shono M, Cho G, Yasui M, Agre P, Nielsen S. Identification of AQP5 in lipid rafts and its translocation to apical membranes by activation of M3 mAChRs in interlobular ducts of rat parotid gland. *Am J Physiol Cell Physiol* 2005;289:1303–1311.
31. Kuroha M, Son DS, Shimoda M. Effects of altered plasma α1 acid glycoprotein levels on pharmacokinetics of some basic antibiotics in pigs: simulation analysis. *J Vet Pharmacol Ther* 2001;24:423–431.
32. Li Y, Azuma A, Takahashi S, Usuki J, Matsuda K, Aoyama A, Kudoh S. Fourteen-membered ring macrolides inhibit vascular cell adhesion molecule 1 messenger RNA induction and leukocyte migration: role in preventing lung injury and fibrosis in bleomycin-challenged mice. *Chest* 2002;122:2137–2145.
33. Fournier T, Medjoubi-N N, Porquet D. Alpha-1-acid glycoprotein. *Biochim Biophys Acta* 2000;1482:157–171.
34. Fernandes PB, Hardy DJ, McDaniel D, Hanson CW, Swanson RN. In vitro and in vivo activities of clarithromycin against Mycobacterium avium. *Antimicrob Agents Chemother* 1989;33:1531–1534.
35. Conte JE Jr, Golden JA, Duncan S, McKenna E, Zurlinden E. Intrapulmonary pharmacokinetics of clarithromycin and of erythromycin. *Antimicrob Agents Chemother* 1995;39:334–338.
36. Kawashima M, Tatsunami J, Fukuno Y, Nagata M, Tominaga M, Hayashi S. Inhibitory effects of 14-membered ring macrolides antibiotics on bleomycin-induced acute lung injury. *Lung* 2002;180: 73–89.
37. Desaki M, Takizawa H, Ohtoshi T, Kasama T, Kobayashi K, Sunazuka T, Omura S, Yamamoto K, Ito K. Erythromycin suppresses nuclear factor-κB and activator protein-1 activation in human bronchial epithelial cells. *Biochem Biophys Res Commun* 2000;267:124–128.
38. Crestani B, Rolland C, Lardeux B, Fournier T, Bernuau D, Pous C, Vissuzaine C, Li L, Aubier M. Inducible expression of the α1-acid glycoprotein by rat and human type II alveolar epithelial cells. *J Immunol* 1998;160:4596–4605.
39. Fournier T, Bouach N, Delafosse C, Crestani B, Aubier M. Inducible expression and regulation of the alpha 1-acid glycoprotein gene by alveolar macrophages: prostaglandin E2 and cyclic AMP act as new positive stimuli. *J Immunol* 1999;163:2883–2890.
40. Van Den Heuvel MM, Poland DC, De Graaff CS, Hoefsmit EC, Postmus PE, Beelen RH, Van Dijk W. The degree of branching of the glycans of α_1-acid glycoprotein in asthma: a correlation with lung function and inflammatory parameters. *Am J Respir Crit Care Med* 2000;161:1972–1978.

Prediction of Prognosis for Acute Respiratory Distress Syndrome with Thin-Section CT: Validation in 44 Cases[1]

Kazuya Ichikado, MD, PhD
Moritaka Suga, MD, PhD
Hiroyuki Muranaka, MD, PhD
Yasuhiro Gushima, MD, PhD
Hisako Miyakawa, MD, PhD
Mitsuko Tsubamoto, MD, PhD
Takeshi Johkoh, MD, PhD
Naomi Hirata, MD, PhD
Takeshi Yoshinaga, MD
Yoshihiro Kinoshita, MD, PhD
Yasuyuki Yamashita, MD, PhD
Yutaka Sasaki, MD, PhD

Purpose: To retrospectively evaluate whether the thin-section computed tomographic (CT) appearance has prognostic value for prediction of mortality, number of ventilator-free days (ie, days without mechanical ventilation), and 28-day risk of barotrauma in patients with a clinically early stage of acute respiratory distress syndrome (ARDS) from diverse causes.

Materials and Methods: Institutional review board approval and informed consent were obtained. Two independent observers who were blinded to patient outcomes retrospectively evaluated the thin-section CT scans obtained within 7 days after clinical ARDS onset in 26 survivors and 18 nonsurvivors. Of 44 patients, there were 37 men and seven women (mean age ± standard deviation, 61.8 years ± 15.6). CT findings were graded on a scale of 1–6 that corresponded with consecutive pathologic phases: score of 1, normal attenuation; score of 2, ground-glass attenuation; score of 3, consolidation; score of 4, ground-glass attenuation associated with traction bronchiolectasis or bronchiectasis; score of 5, consolidation associated with traction bronchiolectasis or bronchiectasis; and score of 6, honeycombing. An overall CT score was obtained by adding the six averaged scores (three zones in each lung). Multivariate regression analysis was used to assess the independent predictive value of the CT score.

Results: The area of increased attenuation associated with traction bronchiolectasis or bronchiectasis ($P = .002$), as well as the overall CT score ($P = .002$), was smaller in survivors than in nonsurvivors. Results of multivariate regression analysis revealed that CT score was independently associated with mortality ($P = .006$). A CT score of less than 230 enabled prediction of survival with 73% sensitivity and 75% specificity and was associated with both a greater number of ventilator-free days ($P = .018$) and a lower incidence of barotrauma ($P = .013$) within 28 days after ARDS onset.

Conclusion: Extensive thin-section CT abnormalities indicative of fibroproliferative changes were independently predictive of poor prognosis in patients with a clinically early stage of ARDS.

[1] From the Dept of Respiratory Medicine (K.I., M.S., H. Muranaka, H. Miyakawa, Y.S.), Div of Intensive Care Unit (Y.G., Y.K.), and Dept of Diagnostic Radiology (Y.Y.), Graduate School of Medical Sciences, Kumamoto Univ, Kumamoto, Japan; Div of Respiratory Medicine, Saiseikai Kumamoto Hosp, 5-3-1 Chikami, Kumamoto 861-4193, Japan (K.I., M.S., H. Muranaka); Dept of Radiology, Osaka Univ Graduate School of Medicine, Osaka, Japan (M.T., T.J.); and Pulmonary Div, Kumamoto Chu-oh Hosp, Kumamoto, Japan (N.H., T.Y.). Received Sept 4, 2004; revision requested Nov 3; revision received Dec 29; accepted Feb 1, 2005.

Acute respiratory distress syndrome (ARDS) is characterized by the sudden onset of hypoxemia and the appearance of bilateral opacities on chest radiographs in the absence of clinical evidence of left atrial hypertension. It is the most severe form of a wide spectrum of pathologic conditions designated as acute lung injury (1,2). Although the mortality rate for patients with ARDS is 40%–60% (2,3), the prognosis for affected individuals depends on various background factors and on the general severity of underlying or extrapulmonary disease. Results of multivariate regression analyses have revealed an association of death from ARDS with age (>70 years) (4), underlying liver cirrhosis (5), Acute Physiology and Chronic Health Evaluation II (APACHE II) score, and Sequential Organ Failure Assessment (SOFA) score (6). Two pulmonary factors independently associated with mortality are *(a)* direct lung injury as the cause of ARDS and *(b)* the extent of oxygenation impairment on day 3 after the onset of ARDS (5,6).

Thin-section computed tomographic (CT) findings have been reported to be of substantial diagnostic value in ARDS (7–12). To our knowledge, however, no study has been performed to evaluate the prognostic implication of thin-section CT findings. Ichikado et al (13,14) previously showed that thin-section CT findings correlated well with pathologic phases of diffuse alveolar damage, the pathologic hallmark of ARDS, and that assessment with thin-section CT was helpful in predicting prognosis in individuals with acute interstitial pneumonia, an idiopathic form of ARDS, regardless of the severity of the physiologic abnormality (15). Thin-section CT scans of acute interstitial pneumonia obtained in nonsurvivors thus showed more extensive areas of increased attenuation associated with traction bronchiectasis, which corresponded to fibroproliferative phases of diffuse alveolar damage, than did those obtained in survivors.

Given that acute interstitial pneumonia occurs in previously healthy individuals with no underlying disease, most patients with this condition experience respiratory failure but do not experience any of the other organ failures that are associated with preexisting disease (16,17). It was therefore unclear whether the findings in patients with acute interstitial pneumonia would also apply to those with other forms of ARDS. Thus, the aim of the present study was to retrospectively evaluate whether the thin-section CT appearance has prognostic value in the prediction of mortality, the number of ventilator-free days (ie, days without mechanical ventilation), and the 28-day risk of barotrauma in patients with a clinically early stage of ARDS from diverse causes.

Materials and Methods

Patients

Cases of 63 patients with ARDS diagnosed according to the American-European Consensus Conference Criteria (1) were recorded at our institutions between January 2001 and December 2002. This study was approved by the institutional review boards at all institutions, and informed consent was obtained either from the participants or from their families if the participants were unable to decide by themselves. At our institutions, informed consent also included permission for future retrospective analyses. Forty-four (70%) of the 63 patients who had undergone thin-section CT within 7 days after the onset of ARDS were included in the present retrospective study. Patients were excluded if they were younger than 16 years of age, if they could not undergo thin-section CT because of unstable clinical status, if they had chronic interstitial pneumonia, or if they had undergone mechanical ventilation for more than 7 days. These 37 men and seven women (age range, 16–83 years; mean age, 61.8 years ± 15.6 [standard deviation]) had acute respiratory failure from various causes and bilateral opacities seen on conventional chest radiographs without clinical evidence of left atrial hypertension. All 44 patients had moderate-to-severe Murray lung injury scores (range, 2.5–4.0; median, 3.5 ± 0.7) (18) and required mechanical ventilation.

The general severity of disease was assigned an APACHE II score (median, 16.0 ± 4.8). The extent of multiple organ failure was evaluated by means of the SOFA score (median, 5.0 ± 3.1). Documented preexisting diseases were recorded, and underlying medical conditions were classified by means of severity according to the criteria of McCabe and Jackson (19) as nonfatal (score of 1), ultimately fatal (score of 2), or fatal (score of 3).

Ventilator management at the time of the thin-section CT examination was designed to limit plateau pressure at 30 cm H_2O or less, with positive end-expiratory pressure of 5–8 cm H_2O. We recorded the number of ventilator-free days, which were defined as days during which the patient was alive and free from mechanical ventilation, during the first 28 days after the onset of ARDS (K.I., H. Muranaka, Y.G., H. Miyakawa, M.T., N.H.). Barotrauma, which was defined as any new pneumothorax, pneumomediastinum, or subcutaneous emphysema, was noted as present or absent on routine chest radiographs during the first 28 days. The informa-

Published online before print
10.1148/radiol.2373041515

Radiology 2006; 238:321–329

Abbreviations:
APACHE II = Acute Physiology and Chronic Health Evaluation II
ARDS = acute respiratory distress syndrome
ROC = receiver operating characteristic
SOFA = Sequential Organ Failure Assessment

Author contributions:
Guarantors of integrity of entire study, M.S., T.J., Y.K., Y.Y.; study concepts/study design or data acquisition or data analysis/interpretation, all authors; manuscript drafting or manuscript revision for important intellectual content, all authors; approval of final version of submitted manuscript, all authors; literature research, K.I., M.T., N.H.; clinical studies, K.I., H. Muranaka, Y.G., H. Miyakawa, M.T., N.H., T.Y., Y.K.; statistical analysis, K.I.; and manuscript editing, K.I., M.S., T.J., T.Y., Y.Y., Y.S.

Address correspondence to K.I.
(e-mail: *k-ichikado@skh.saiseikai.or.jp*).

Authors stated no financial relationship to disclose.

tion on barotrauma occurrence was obtained from the radiographic reports.

Sepsis surveillance was incorporated into the routine examinations of cultures of blood, urine, and sputum obtained with a sterile intratracheal suction tube. If necessary, bronchoscopy with or without mini-bronchoalveolar lavage was performed.

Although the use of high-dose corticosteroids for the treatment of ARDS is controversial in Japan, it has been shown to be effective (20–22). Two different regimens were used by 21 individual physicians at our institutions, on the basis of their own decisions. Twenty-eight (64%) of 44 patients underwent treatment with high-dose intravenously administered corticosteroids (methylprednisolone, 1–2 grams per day) for 3-day periods, with adequate antibiotic therapy. Ten of the remaining 16 patients were treated with intravenously administered low-dose methylprednisolone (2 mg per kilogram of body weight per day) (23), whereas corticosteroid therapy was contraindicated in the remaining six patients because of gastrointestinal bleeding. In each group of patients treated with methylprednisolone, the dose of corticosteroid was gradually reduced over 1–2 months. Twenty-six (59%) of 44 patients responded to medical treatment and survived, and the remaining 18 patients died of multiorgan failure (n = 13) or respiratory failure (n = 5) within 1 week to 2 months despite intensive treatment.

CT Examination

All patients underwent thin-section CT of the chest once within 7 days (mean, 2.1 days ± 1.5) after the onset of ARDS. CT was performed with various CT scanners. The thin-section CT scans consisted of 1-mm-collimation sections reconstructed with the use of a high-spatial-frequency algorithm. Sections were obtained at 10-mm intervals throughout the chest with the patient in the supine position and without intravenous contrast medium. To avoid degradation of thin-section CT scans by respiratory motion in patients undergoing mechanical ventilation, when CT was performed, full inspiration was sustained by using a respiratory bag with a Jackson-Rees expiration valve (Igarashi Ika-kohgyo, Tokyo, Japan). None of the patients experienced a deterioration in condition as a result of undergoing the CT examination.

Thin-Section CT Scan Assessment

Thin-section CT scans were evaluated by two independent observers (M.T., T.J.) with more than 10 years of experience in thin-section CT interpretation who were unaware of patient outcome. The observers assessed the presence and extent of areas of ground-glass attenuation, airspace consolidation, traction bronchiectasis, traction bronchiolectasis, and honeycombing. Ground-glass attenuation was defined as an area of hazy increased opacification without obscuration of underlying vascular markings. Airspace consolidation was considered present when the vascular markings were obscured. When bronchi were irregular in contour, the dilated bronchus within areas of parenchymal abnormality was recognized as traction bronchiectasis. Traction bronchiolectasis was identified by means of the presence of dilated bronchioles within areas with parenchymal abnormality. Architectural distortion was defined as the presence of displacement or distortion of interlobar fissures, interlobular septa, bronchi, or vessels. Interlobular septal thickening was recognized as abnormal thickening of interlobular septa. Intralobular interstitial thickening was identified by means of a fine reticular, or meshlike, appearance to the lung parenchyma. Honeycombing was defined as the presence of cystic air spaces measuring 2–10 mm in diameter with well-defined walls.

Scoring of Thin-Section CT Findings

The thin-section CT findings were graded on a scale of 1–6 on the basis of the classification system previously described (15): score of 1, normal attenuation; score of 2, ground-glass attenuation; score of 3, consolidation; score of 4, ground-glass attenuation with traction bronchiolectasis or bronchiectasis; score of 5, consolidation with traction bronchiolectasis or bronchiectasis; and score of 6, honeycombing. The presence of each of these six abnormalities was assessed independently in three (upper, middle, and lower) zones of each lung. The upper zone was defined as the area above the level of the carina, the middle zone as the area between the level of the carina and the level of infrapulmonary vein, and the lower zone as the area below the level of infrapulmonary vein. The extent of each abnormality was determined by visually estimating the percentage (to the nearest 10%) of the affected lung parenchyma in each zone. The assessments of the two observers were averaged. The abnormality score for each zone was calculated by multiplying the percentage area by the point value (the score of 1–6). The six zone scores were averaged to determine the total score for each abnormality in each patient. The overall CT score for each patient was obtained by adding the six averaged scores.

Statistical Analysis

Data are expressed as mean ± standard deviation, unless indicated otherwise. Interobserver variability in identification of parenchymal abnormalities on the CT scans was assessed with the κ statistic. Interobserver variability in estimation of the extent of each finding was assessed with the Spearman rank correlation coefficient. Differences in CT findings between survivors and nonsurvivors were analyzed by using the χ^2 test or the Fisher exact test. Comparison of CT score between survivors and nonsurvivors was evaluated by means of the Mann-Whitney U test.

To analyze the CT score as a predictor of survival, of the failure of ventilator weaning, or of the occurrence of barotrauma within 28 days after the onset of ARDS, we used receiver operator characteristic (ROC) curves to determine the cutoff value of the CT score that yielded the highest sensitivity and specificity (24). We also evaluated the relation between the cutoff CT score and the number of ventilator-free days within 28 days after the onset of ARDS. Analyses of the ROC were computed

Table 1

Clinical Characteristics of Patients with ARDS at Time of CT Examination

Characteristic	All Patients ($n = 44$)	Survivors ($n = 26$)	Nonsurvivors ($n = 18$)	*P* Value*
Age (y)†	61.8 ± 15.6	59.4 ± 14.1	65.2 ± 17.4	.087
Sex				NS
Male	37	23	14	
Female	7	3	4	
Liver cirrhosis (%)	15.9	16.3	15.6	NS
Direct/indirect injury	19/25	11/15	8/10	NS
Pneumonia (%)	36	35	39	NS
Sepsis (%)	16	15	17	NS
Aspiration (%)	7	8	6	NS
Postoperative (%)	7	4	11	NS
Drug related (%)	7	11	0	NS
Near drowning (%)	5	8	0	NS
Pancreatitis (%)	2	0	5	NS
Unknown (%)	20	19	22	NS
Time from onset (d)†	2.1 ± 1.5	1.7 ± 1.1	2.6 ± 1.8	NS
Lung injury score‡	3.5 ± 0.7	3.5 ± 0.6	3.3 ± 0.7	NS
APACHE II score‡	16.0 ± 4.8	15.0 ± 4.2	17.0 ± 5.4	NS
SOFA score‡	5.0 ± 3.1	5.0 ± 2.9	6.0 ± 3.3	NS
McCabe score				.070
1	33	22	11	
2	7	3	4	
3	4	1	3	
Steroid therapy				
High dose	28	14	14	NS
Low dose	10	8	2	NS
None	6	4	2	NS

Note.—Unless otherwise indicated, data are numbers of patients.

* *P* values refer to comparisons between survivors and nonsurvivors. NS = not significant.

† Data are mean ± standard deviation.

‡ Data are median ± standard deviation.

Table 2

Thin-Section CT Findings in Survivors and Nonsurvivors of ARDS

CT Finding	Survivors ($n = 26$)	Nonsurvivors ($n = 18$)
Architectural distortion	15 (58)	15 (83)
Traction bronchiolectasis or bronchiectasis	14 (54)	14 (78)
Intralobular interstitial thickening	12 (46)	8 (44)
Interlobular septal thickening	14 (54)	9 (50)
Honeycombing	0 (0)	0 (0)
Ground-glass attenuation	25 (96)	18 (100)
Air-space consolidation	24 (92)	17 (94)

Note.—Data are numbers of patients, and data in parentheses are percentages. No significant differences were apparent between the groups.

with a computer program (LABROC4, IBM compatible version, 1999; C. E. Metz, University of Chicago, Chicago, Ill). Multivariate regression analysis was used to assess the independent predictive value of the CT score.

To evaluate whether the number of days from the onset of ARDS really correlated with the histopathologic stages of ARDS, the relation between the thin-section CT score and the disease duration of ARDS was assessed with the Spearman rank correlation coefficient. Statistical analyses were performed by using a commercially available software package (SPSS, version 12.0J; SPSS, Chicago, Ill). For all statistical analyses, $P < .05$ was considered to indicate a significant difference.

Results

Baseline Clinical Characteristics

The demographic data, causes of ARDS, and clinical variables on the day of thin-section CT scanning for all 44 study patients, as well as those of the survivors and nonsurvivors, are shown in Table 1. Survivors tended to be younger and to have more favorable prognoses of underlying diseases, as shown by smaller McCabe scores, than did nonsurvivors, but no significant differences were seen between the two groups.

Thin-Section CT Findings in Survivors and Nonsurvivors

The frequency of each CT finding in survivors and nonsurvivors is summarized in Table 2. Traction bronchiolectasis or bronchiectasis and architectural distortion tended to be less common in survivors than in nonsurvivors, but these differences were not statistically significant. The area of increased attenuation associated with traction bronchiolectasis or bronchiectasis was significantly smaller in survivors than in nonsurvivors (Table 3, Fig 1), whereas the area of increased attenuation without traction bronchiolectasis or bronchiectasis was greater in survivors than in nonsurvivors (Fig 2). The extent of other parenchymal abnormalities did not differ significantly between survivors and non-

Table 3

Extent of Each CT Finding in Survivors and Nonsurvivors of ARDS

CT Finding	Survivors ($n = 26$)	Nonsurvivors ($n = 18$)	*P* Value*
Spared area	28.0 ± 14.7	24.1 ± 18.0	NS
Ground-glass attenuation	42.7 ± 21.1	21.8 ± 22.0	.001
Airspace consolidation	19.6 ± 16.6	12.2 ± 15.7	.070
Total area without traction bronchiolectasis or bronchiectasis	90.3 ± 15.5	58.1 ± 32.8	.002
Ground-glass attenuation plus traction bronchiolectasis or bronchiectasis	6.7 ± 11.4	32.2 ± 30.5	.004
Airspace consolidation plus traction bronchiolectasis or bronchiectasis	2.9 ± 4.8	9.5 ± 15.3	.10
Total area with traction bronchiolectasis or bronchiectasis	9.6 ± 15.5	41.8 ± 32.8	.002
Honeycombing	0.0 ± 0.0	0.0 ± 0.0	NS

Note.—Data are mean ± standard deviation of percentage of lung involvement.

* NS = not significant.

Figure 1

Figure 1: Thin-section CT scans at the level of the carina obtained in a 76-year-old man on the day of ARDS onset from viral pneumonia (P_{AO_2}/F_{IO_2} score, 121 mm Hg). Scan shows ground-glass attenuation associated with traction bronchiectasis (arrows) and fine reticular opacities. Overall thin-section CT score is 311. This patient needed ventilator assistance for more than 28 days.

Figure 2

Figure 2: Thin-section CT scan at the level of the right infrapulmonary vein obtained in a 51-year-old woman on the day of ARDS onset from bacterial pneumonia (P_{AO_2}/F_{IO_2} score, 123 mm Hg). Scan shows extensive airspace consolidation without traction bronchiectasis. Bronchial walls are smooth and not dilated, as indicated by regularity along the wall length. Pleural effusion is not apparent. Overall thin-section CT score is 217. This patient was weaned from mechanical ventilation 11 days after onset of ARDS.

Figure 3

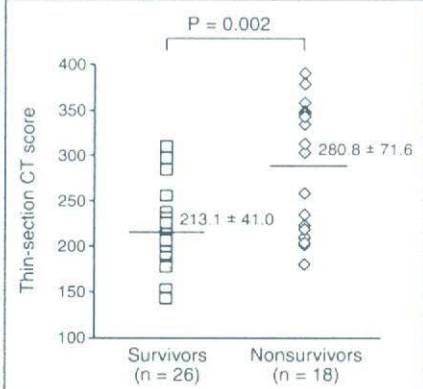

Figure 3: Graph compares thin-section CT scores between survivors and nonsurvivors of ARDS. CT score was significantly lower in patients who survived than in those who died ($P = .002$).

survivors. The interobserver variability in evaluation of the presence of lung abnormalities was good (κ value, 0.68–0.82), and the assessments of the extent of abnormalities made by the two different observers were also well correlated (Spearman rank correlation coefficient, 0.72; $P < .01$).

Prognostic Value of the CT Score

The overall CT score in survivors (mean, 213.1 ± 41.0; range, 143.4–310.5) was significantly lower than that in nonsurvivors (mean, 280.8 ± 71.6; range, 180.1–390.4) (Fig 3). Construction of an ROC curve yielded an optimal cutoff value of a CT score of 230 for prediction of survival, with a sensitivity of 73% and a specificity of 75% (Fig 4). Multivariate regression analysis, with adjustment for demographic characteristics, general severity, and underlying disease condition, revealed that the CT score was independently associated with mortality ($R^2 = 0.436$), with an odds ratio of 4.7 when expressed as mortality change per 10% increase in area of attenuation with traction bronchiolectasis or bronchiectasis on thin-section CT scans (Table 4).

CT Score and Number of Ventilator-Free Days or Incidence of Barotrauma

Patients with a CT score of less than 230 had a significantly higher number of ventilator-free days (13.7 days ± 10.6 vs 5.7 days ± 9.7, $P = .018$) and a significantly lower incidence of barotrauma (3.8% vs 33.3%, $P = .013$) within 28 days after the onset of ARDS than did those with an CT score of 230 or higher. Five of seven patients with barotrauma had pneumothorax, and the other two patients had pneumomediastinum. Barotrauma occurred 14–21 days (mean, 16.3 days ± 2.6) after the onset of ARDS. An ROC curve was used to identify the optimal cutoff value of a CT score of 247 for the prediction of the onset of barotrauma, with a sensitivity of 66% and a specificity of 75% (Fig 5). Another ROC curve was used to determine the best cutoff value of a CT score of 230 for the prediction of the failure of ventilator weaning within 28 days, with a sensitivity of 73% and a specificity of 76% (area under the ROC curve, 0.820).

CT Score and Disease Duration

Despite the short time (mean, 2.1 days ± 1.5) that had elapsed between the onset of ARDS and CT examination, 28 (64%) of the 44 patients manifested areas of increased attenuation associated with traction bronchiolectasis or bronchiectasis on CT scans, which was indicative of the fibroproliferative phase of diffuse alveolar damage (Fig 1). The CT score was significantly but weakly (Spearman rank correlation coefficient, 0.33; $P = .03$) associated with the number of days since the onset of ARDS (Fig 6).

Figure 4

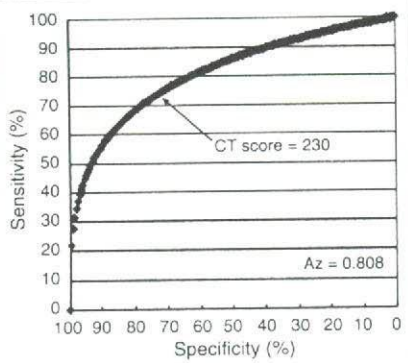

Figure 4: ROC curve of prognostic value of the CT score identified the optimal cutoff value of 230 for prediction of survival, with 73% sensitivity and 75% specificity. Area under the ROC curve *(Az)* indicates an index of discrimination performance for survival is 0.808.

Figure 5

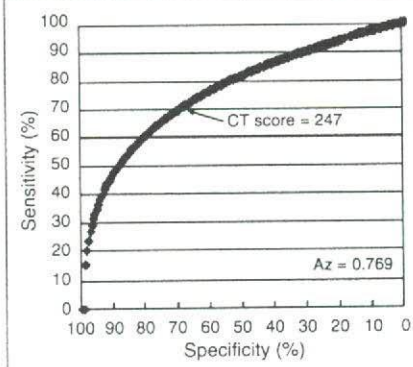

Figure 5: ROC curve for the prediction of the onset of barotrauma from CT score identified the optimal cutoff value of 247 for prediction of barotrauma onset with 66% sensitivity and 75% specificity. Area under the ROC curve *(Az)* indicates an index of discrimination performance for the occurrence of barotrauma is 0.769.

Discussion

We have evaluated the prognostic implication of thin-section CT assessment by determining the extent of fibroproliferation diagnosed at imaging in patients in the early stage of ARDS from diverse causes. We found that the thin-section CT score obtained within a week after the onset of ARDS was an independent predictive factor for survival with multivariate analysis; the survival rate of patients in whom thin-section CT scans showed extensive abnormalities indicative of the fibroproliferative phase of diffuse alveolar damage was thus lower than that of patients in whom such changes were less marked. Ichikado et al (13,14) previously demonstrated a close correlation between thin-section CT findings and the pathologic phase of diffuse alveolar damage. In these previous studies, the areas of increased at-

Table 4

Multiple Logistic Regression Analysis of Variables Potentially Associated with Mortality in Patients with ARDS

Variable	*P* Value	Odds Ratio	95% Confidence Interval
CT score	.006	4.7*	1.009, 1.054
Lung injury score	.034	0.2†	0.031, 0.871
Liver cirrhosis	.155		
Age > 70 years	.188		
APACHE II score	.256		
McCabe score	.406		
SOFA score	.852		
Direct injury	.952		

* Expressed as mortality change per 10% increase in area of attenuation with traction bronchiolectasis or bronchiectasis on thin-section CT scans.

† Expressed as mortality change per one point increase in lung injury score.

Figure 6

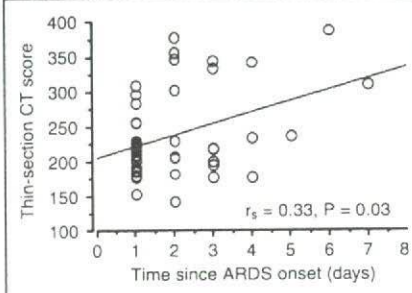

Figure 6: Graph shows correlation between CT score and number of days elapsed since onset of ARDS in the 44 patients. CT score was significantly but weakly correlated with number of days since onset of ARDS. Note that high CT scores were observed in some cases even on the day of ARDS onset.

tenuation (ground-glass attenuation or airspace consolidation) without traction bronchiolectasis or bronchiectasis on thin-section CT scans corresponded to histologic features of the exudative or early proliferative phase of diffuse alveolar damage, whereas the presence of traction bronchiolectasis or bronchiectasis in areas of ground-glass attenuation or consolidation was associated with the late proliferative or fibrotic phase of such damage. The authors have also previously showed that assessment at thin-section CT was a prognostic factor for patients with acute interstitial pneumonia irrespective of the underlying physiologic abnormality (15).

In contrast to acute interstitial pneumonia, which affects previously healthy individuals, has an unknown cause, and is a "pure" form of acute respiratory failure, ARDS is generally associated with a variety of causes and is often associated with the failure of other organs that results from various underlying diseases (5,6,16,17). Multivariate regression analyses of baseline risk factors for survival have shown that an age older than 70 years (4), the presence of liver cirrhosis as an underlying disease (5), a high McCabe score for prognosis of the underlying disease, and a high APACHE II score are independently associated with mortality. The SOFA score is also an important predictor of survival (5,6). As far as we are aware, however, few pulmonary factors have been associated with ARDS mortality; those factors so associated include direct lung injury as the cause of ARDS and the extent of oxygenation impairment on day 3 after the onset of ARDS (5). Our present data suggest that the thin-section CT score defined herein provides information about the histopathologic stage of ARDS and that this score might be informative with regard to the response to treatment. However, in contrast to the high specificity and sensitivity (for prediction of survival with the optimal cutoff CT score) in acute interstitial pneumonia (15), the low specificity (75%) and sensitivity (73%) values for prediction of survival with the optimal cutoff CT score of 230 suggest that extrapulmonary or multiorgan disease factors affect prognosis even in individuals with a high CT score.

In a previous study (25) of 45 cases of ARDS confirmed at biopsy, patients whose condition was shown histologically to be in the acute exudative phase had a better prognosis than did those whose condition was shown to be in more advanced phases. Authors of other studies that have involved histologic analysis of specimens obtained by means of open lung biopsy have suggested that low-dose and prolonged corticosteroid treatment improves survival, especially when administered in the early proliferative phase of ARDS (23,26–28). In the present study, the group of patients who had mostly exudative lesions and limited areas of thin-section CT abnormalities indicative of the fibroproliferative phase (CT score, <230) had a lower mortality than did both the patients who had more extensive areas of fibroproliferation (CT score, ≥230). These results suggest a possible relationship between the pathologic stage of diffuse alveolar damage and responsiveness to corticosteroid treatment. Prospective studies with a larger number of patients are required to confirm such a relation.

In the present study, traction bronchiolectasis or bronchiectasis was already apparent on thin-section CT scans obtained within a few days of ARDS onset in 28 (64%) of 44 patients. Howling et al (29), on the basis of a review of thin-section CT findings in 16 patients with early phase ARDS, reported that bronchiectasis associated with ground-glass attenuation was a frequent observation that tended to persist at follow-up and was usually accompanied by the CT finding of supervening fibroproliferation. The CT score in our patients was weakly correlated with time elapsed since ARDS onset. A clinically early time point therefore does not necessarily correspond to a pathologically early phase of ARDS.

Johkoh et al (30), on the basis of their evaluation of 36 patients with idiopathic ARDS, or acute interstitial pneumonia, reported that the extent of traction bronchiectasis, which evolved from bronchioles to central bronchi with the extent of fibroproliferation, was weakly correlated with disease duration and suggested that difficulty in determination of the onset of injury might explain the weak correlation between them. Given that no significant difference in the cause of ARDS was apparent between the survivors and nonsurvivors in the present study, the weakness of the correlation between the CT score and the clinical duration of ARDS may also be attributable to differences in individual sensitivity to lung injury and in the intensity of the consequent exaggerated inflammation that occurs between the onset of lung injury and progression to ARDS. In the present study, if only the parameter of time elapsed since onset of ARDS was used to identify disease stage, some patients with fibroproliferative changes would be diagnosed with early ARDS (Fig 6). Such a situation might explain the discrepancy in the effectiveness of treatment between patients with "clinically" early phases of ARDS and those with "pathologically" early phases of ARDS.

In the current study, the thin-section CT score showed a significant inverse association with the number of ventilator-free days. Prolonged ventilation has been found to contribute to systemic inflammation and multiple organ failure in patients with ARDS (29). In our study, the death of 13 of the 18 nonsurvivors with ARDS, who required prolonged ventilation, was associated with multiple organ failure. A reduction in the duration of ventilation should therefore result in a reduction in ventilator-associated lung injury and thereby improve survival (31,32). Given that the patients in our study with lower CT scores needed less ventilator assistance than did those with higher CT scores, the former individuals may have experienced a reduced extent of ventilator-induced lung injury and therefore had an improved survival rate.

Barotrauma was more frequent in patients with a higher CT score (score ≥ 230) than in those with a lower CT score (score < 230) during the first 28 days after the onset of ARDS. Barotrauma occurred more than 14 days af-

ter ARDS onset. Most barotrauma events have also previously been shown to occur late in the course of ARDS and to be related to lung structural changes, such as emphysemalike or fibroproliferative lesions that develop over time (33). Desai et al (7) also reported that a coarse reticular pattern with distortion of lung parenchyma on the follow-up thin-section CT scans correlated well with the total duration of mechanical ventilation. Given that a higher CT score at presentation is indicative of more advanced fibroproliferative changes, our data may support those of these previous studies and suggest that thin-section CT findings might be used as a predictor of barotrauma in the development of therapeutic strategies for lung protection.

There were some potential limitations in the present study. Our study was retrospective and included only 44 patients who had undergone thin-section CT scanning within 7 days after the onset of ARDS; thus, although it included 70% of the patients with ARDS at our institutions during the allotted time period, our study may have a case selection bias and may not sufficiently reflect all forms of ARDS. Furthermore, in the present study, no correlation was provided with either physiologic parameters or pathologic correlation. Further prospective evaluation of thin-section CT findings in patients with ARDS will be necessary not only to clarify their prognostic implications but also to assess their potential application in the development of treatment strategies based on pathologic stage. Ideally, such investigations would also help determine the most appropriate time for administration of pharmacologic agents, such as corticosteroids.

In summary, thin-section CT findings suggestive of extensive fibroproliferative changes are independently predictive of poor prognosis in patients with clinically early ARDS. Such findings also are associated with a longer duration of ventilator assistance and a higher frequency of barotrauma during the first 28 days after the onset of ARDS. We conclude that the accurate determination of disease stage by means of thin-section CT assessment is informative with regard to the potential for ventilator-induced lung injury and the response to treatment in individuals with ARDS.

Acknowledgment: We thank Shigehiko Katsuragawa, MD, PhD, Kumamoto University School of Health Sciences, for suggestions on statistical methodology.

References

1. Bernard GR, Artigas A, Brigham KL, et al. The American-European consensus conference on ARDS: definitions, mechanisms, relevant outcomes, and clinical trial coordination. Am J Respir Crit Care Med 1994;149:818–824.
2. Ware LB, Matthay MA. The acute respiratory distress syndrome. N Engl J Med 2000;342:1334–1349.
3. Milberg JA, Davis DR, Steinberg KP, et al. Improved survival of patients with acute respiratory distress syndrome (ARDS): 1983–1993. JAMA 1995;273:306–309.
4. Ely EW, Wheeler AP, Thompson BT, et al. Recovery rate and prognosis in older persons who developed acute lung injury and the acute respiratory distress syndrome. Ann Intern Med 2002;136:25–36.
5. Monchi M, Bellenfant F, Cariou A, et al. Early predictive factors of survival in the acute respiratory distress syndrome: a multivariate analysis. Am J Respir Crit Care Med 1998;158:1076–1081.
6. Estenssoro E, Dubin A, Laffaire E, et al. Incidence, clinical course, and outcome in 217 patients with acute respiratory distress syndrome. Crit Care Med 2002;30:2450–2456.
7. Desai SR, Wells AU, Rubens MB, Evans TW, Hansell DM. Acute respiratory distress syndrome: CT abnormalities at long-term follow-up. Radiology 1999;210:29–35.
8. Desai SR, Wells AU, Suntharalingam G, Rubens MB, Evans TW, Hansell DM. Acute respiratory distress syndrome caused by pulmonary and extrapulmonary injury: a comparative CT study. Radiology 2001;218:689–693.
9. Tomiyama N, Müller NL, Johkoh T, et al. Acute respiratory distress syndrome and acute interstitial pneumonia: comparison of thin-section CT findings. J Comput Assist Tomogr 2001;25:28–33.
10. Desai SR. Acute respiratory distress: imaging of the injured lung. Clin Radiol 2002;57:8–17.
11. Padley SP, Jordan SJ, Goldstraw P, Wells AU, Hansell DM. Asymmetric ARDS following pulmonary resection: CT findings—initial observations. Radiology 2002;223:468–473.
12. Joynt GM, Antonio GE, Lam P, et al. Late-stage adult respiratory distress syndrome caused by severe acute respiratory syndrome: abnormal findings at thin-section CT. Radiology 2004;230:339–346.
13. Ichikado K, Johkoh T, Ikezoe J, et al. Acute interstitial pneumonia: high-resolution CT findings correlated with pathology. AJR Am J Roentgenol 1997;168:333–338.
14. Ichikado K, Suga M, Gushima Y, et al. Hyperoxia-induced diffuse alveolar damage in pigs: correlation between thin-section CT and histopathologic findings. Radiology 2000;216:531–538.
15. Ichikado K, Suga M, Müller NL, et al. Acute interstitial pneumonia: comparison of high-resolution computed tomography findings between survivors and non-survivors. Am J Respir Crit Care Med 2002;165:1551–1556.
16. Hansell DM. Acute interstitial pneumonia: clues from the white stuff. Am J Respir Crit Care Med 2002;165:1465–1466.
17. Quefatieh A, Stone CH, DiGiovine B, et al. Low hospital mortality in patients with acute interstitial pneumonia. Chest 2003;124:554–559.
18. Murray JF, Matthay MA, Luce JM, et al. An expanded definition of the adult respiratory distress syndrome. Am Rev Respir Dis 1988;138:720–723.
19. McCabe WR, Jackson GG. Gram negative bacteremia: etiology and ecology. Arch Intern Med 1962;110:847–852.
20. Yokoyama T, Sakamoto T, Shida N, et al. Bacteremic and leukopenic pneumococcal pneumonia: successful treatment with antibiotics, pulse steroid, and continuous hemodiafiltration. J Infect Chemother 2002;8:247–251.
21. Kamijo Y, Soma K, Asari Y, et al. Pulse steroid therapy in adult respiratory distress syndrome following petroleum naphtha injection. J Toxicol Clin Toxicol 2000;38:59–62.
22. Tamura S, Koreeda T, Nakano T, et al. A case of rheumatoid arthritis which developed after recovery from adult respiratory distress syndrome. Jpn J Med 1990;29:611–615.
23. Meduri GU. Effect of prolonged methylprednisolone therapy in unresolving acute respiratory distress syndrome: a randomized controlled trial. JAMA 1998;280:159–165.
24. Metz CE. ROC methodology in radiologic imaging. Invest Radiol 1986;21:720–733.

25. Lamy M, Fallat RJ, Koeniger E, et al. Pathologic features and mechanisms of hypoxemia in adult respiratory distress syndrome. Am Rev Respir Dis 1976;114:267–284.

26. Meduri GU, Chinn AJ, Leeper KV, et al. Corticosteroid rescue treatment of progressive fibroproliferation in late ARDS: patterns of response and predictors of outcome. Chest 1994;105:1516–1527.

27. Meduri GU, Belenchia JM, Estes RJ, et al. Fibroproliferative phase of ARDS: clinical findings and effects of corticosteroids. Chest 1991;100:943–952.

28. Bloomfield R, MacMillan M, Noble DW. Corticosteroid insufficiency in acutely ill patients. N Engl J Med 2003;348:2157–2159.

29. Howling SJ, Evans TW, Hansell DM. The significance of bronchial dilatation on CT in patients with adult respiratory distress syndrome. Clin Radiol 1998;53:105–109.

30. Johkoh T, Müller NL, Taniguchi H, et al. Acute interstitial pneumonia: thin-section CT findings in 36 patients. Radiology 1999; 211:859–863.

31. Pinhu L, Whitehead T, Evans T, et al. Ventilator-associated lung injury. Lancet 2003; 361:332–340.

32. Schoenfeld DA, Bernard GR; for the ARDS Network. Statistical evaluation of ventilator-free days as an efficacy measure in clinical trials of treatments for acute respiratory distress syndrome. Crit Care Med 2002;30: 1772–1777.

33. Gattinoni L, Bombino M, Pelosi P, et al. Lung structure and function in different stages of severe adult respiratory distress syndrome. JAMA 1994;271:1772–1779.